

Lattice gauge theory and topological quantum error correction with quantum deviations in the state preparation and error detection

Yuanchen Zhao¹ and Dong E. Liu^{1,2,3,4,*}

¹*State Key Laboratory of Low Dimensional Quantum Physics,
Department of Physics, Tsinghua University, Beijing, 100084, China*
²*Beijing Academy of Quantum Information Sciences, Beijing 100193, China*
³*Frontier Science Center for Quantum Information, Beijing 100184, China*
⁴*Hefei National Laboratory, Hefei 230088, China*

(Dated: March 29, 2025)

Quantum deviations or coherent noise are a typical type of noise when implementing gate operations in quantum computers, and their impact on the performance of quantum error correction (QEC) is still elusive. Here, we consider the topological surface code, with both stochastic noise and coherent noise on the multi-qubit entanglement gates during stabilizer measurements in both initial state preparation and error detection. We map a multi-round error detection protocol to a three-dimensional statistical mechanical model consisting of \mathbb{Z}_2 gauge interactions and related the error threshold to its phase transition point. Specifically, two error thresholds are identified distinguishing different error correction performances. Below a finite error threshold, in stark contrast to the case with only stochastic errors, unidentifiable measurement errors can cause the failure of QEC in the large code distance limit. This problem can only be fixed at the perfect initial state preparation point. For a finite or small code with distance d , we find that if the preparation error rate is below a crossover scale $\propto 1/\log d$, the logical errors can still be suppressed. We conclude that this type of unavoidable coherent noise has a significant impact on QEC performance, and becomes increasingly detrimental as the code distance increases.

I. INTRODUCTION

Quantum supremacy was recently claimed in cutting-edge quantum processors [1–3], which is a major breakthrough in the field of quantum computation. Because to their noisy character, the current state-of-the-art quantum devices [1–7] are classified as noisy intermediate-scale quantum (NISQ) [8] computer, and the observed quantum supremacy is only a weakened version with few practical applications [8]. To date, the merely known examples with worthwhile quantum advantages are only expected in fault tolerant quantum computers with quantum error correction (QEC) [9–11]. Recently, QEC codes with small system size are being put to the test in experiments [12–22].

A key concept of fault tolerance is the “error threshold theorem”, which states that if the physical error rate is below an error threshold, quantum computation with arbitrary logical accuracy can be in principle implemented in the noisy quantum devices [23–26]. The threshold theorem is well-established if the device noise can be captured by independent stochastic errors [23, 25, 27–29]. However, actual quantum devices suffer from more general type of errors. With correlated errors, the threshold theorem is modified for a more conceptual infidelity measure, e.g. diamond norm [24], for correlations with weak amplitude [30] and weak length [31], and for the environment with critical behaviors [32, 33]. A more practical type of noise comes from the inefficient qubit calibration and imperfect control of gate operations, causing quantum deviation or coherent effect in errors. This problem motivated recent studies for the independent single-qubit coherent errors [34–41]

and the detection induced coherent errors from entanglement gate noise [42, 43]. We emphasize that the two-qubit entanglement gates are much harder to calibrate and more error-prone than single-qubit gate. Nevertheless, the fault-tolerance and error threshold theorem is not established with any kind of coherent errors. Understanding this issue is exceedingly challenging due to the lack of analytical and numerical tools. Although an efficient numerical strategy exists for a special independent coherent error model [36], the general coherent error problems, that goes beyond the Clifford algebra, cannot be simulated efficiently in classical computer. Of that situation, there is no solid foundation for fault-tolerant quantum computation with practical quantum devices. This motivates us to build a theoretical framework to study the coherent error problems in QEC and threshold theorem.

Summary of the main results: In this work, we study the performance of toric code QEC [44] under imperfect measurement while applying the common multi-round syndrome measurements [28], together with the stochastic Pauli errors on physical qubits. We assume that the measurement circuit for both initial state preparation and error detection are suffering from coherent noise. We find that this QEC model can be mapped to a 3D quenched disordered SM model constituted by \mathbb{Z}_2 gauge interaction terms. Remarkably, this model has a non-local correlation term at timelike direction originates from the imperfection during initial state preparation. We further find that the Wilson loops in this SM model have an anisotropic behavior: The timelike Wilson loops deconfine at low temperatures (small physical error rates) and confine at high temperatures (large physical error rates); but the space-like Wilson loops confine at any finite temperature, resulting from the non-local timelike correlation. Taking the results of this SM model, we predict that there are two thresholds in our QEC model. The confinement-deconfinement transition

* Corresponding to: dongeliu@mail.tsinghua.edu.cn

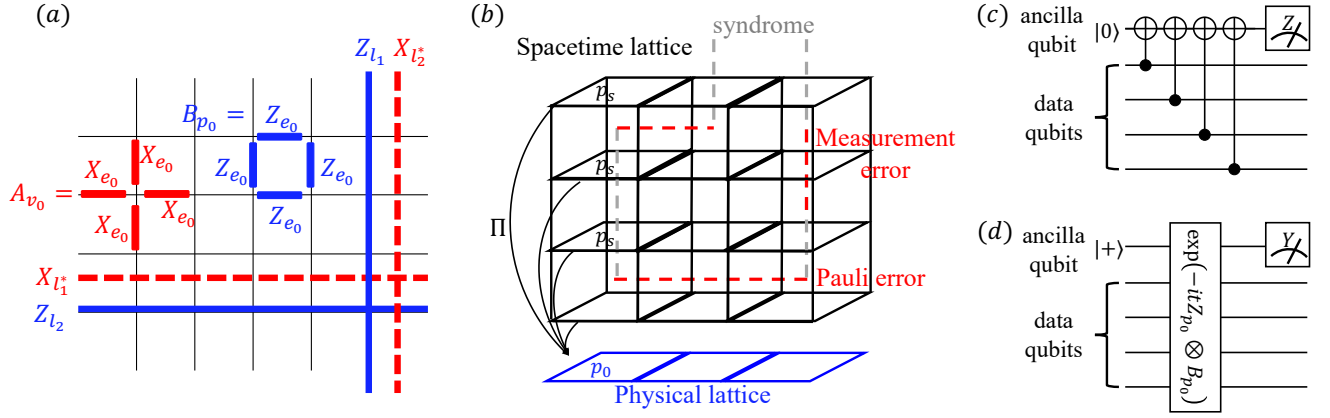


Figure 1. (a) Toric code defined on 2-d periodic lattice. Physical qubits stay on the edges of the lattice. The two kinds of stabilizers are $A_v = \prod_{e|v \in \partial e} X_e$ defined on each vertex and $B_p = \prod_{e \in \partial p} Z_e$ defined on each plaquette as shown in the figure. Logical Pauli Z (X) operators correspond to products of single qubit Z (X) operators along non-contractible loops on the lattice (dual lattice). They satisfy the commutation relations $X_{l_1}^* Z_{l_1} = -Z_{l_1} X_{l_1}^*$, $X_{l_1}^* Z_{l_2} = Z_{l_2} X_{l_1}^*$, $X_{l_2}^* Z_{l_1} = Z_{l_1} X_{l_2}^*$ and acts respectively on two different logical qubits of toric code. (b) 3-d spacetime of error history. The black lattice is the spacetime lattice, which takes periodic boundary condition at space directions and infinity boundary condition at time direction. This boundary condition is also the one adopted in Ref. [27] when discussing SM mapping. The Pauli errors, measurement errors and error syndromes are represented as strings on the dual lattice (dashed lines that cross plaquettes). Given a configuration of Pauli X error (horizontal red strings) for the entire history, the error syndrome (vertical gray strings) will be the configuration of -1 ancilla measurement outcomes at different time steps. The error syndrome is supposed to match the endpoints of Pauli error strings, but due to imperfection of syndrome measurements, the syndrome outcomes might be flipped with certain probability. Those flipped syndromes will be referred to as measurement errors (vertical red strings). Π denotes the projection from the 3-d spacetime lattice to the 2-d physical lattice. Given a plaquette p_s , $\Pi(p_s)$ yields a plaquette p_0 at the same spatial location as p_s . (c) A realistic circuit for B_{p_0} measurement [28]. The ancilla qubit is prepared in $|0\rangle$ state, then four $CNOT$ gates are applied in order to couple data and ancilla qubits. Finally, the ancilla is projectively measured in Z basis. (d) A simplified B_{p_0} measurement circuit considered in our work. Note that a five-qubit unitary gate is used here instead of four two-qubit gates. To enable a theoretical analysis of the problem, we focus on the case (d) in our theory, and the relation between (c) and (d) will be discussed in Sec. VII.

point of timelike Wilson loops signifies a theoretical threshold located at finite measurement error rate and finite Pauli error rate, above which the QEC fails due to non-contractible logical errors. The confinement behavior of spacelike Wilson loops suggests that the measurement error threshold seats at the point where the initial state preparation is perfect. Above the measurement error threshold, if we only take finite error history while decoding, the measurement errors will no longer be distinguished from Pauli errors, which could result in the failure of QEC even in the limit of large code distance. With a finite code distance d , the effectiveness of the pragmatic QEC approach remains viable when the error rate associated with state preparation falls within a region $\sim 1/\log d$. Finally, we emphasize that a more realistic imperfect measurement model relating to Fig. 1(b) will in general has a worse performance, see the discussion of Eq. (27).

II. TORIC CODE—A BRIEF REVIEW

We follow the construction of topological surface code on a torus, i.e. toric code [27–29, 44]. It is a stabilizer code defined on a 2-d periodic square lattice. There are two kinds of stabilizers associated with vertices and plaquettes respectively

as shown in Fig. 1(a),

$$A_{v_0} = \prod_{e_0|v_0 \in \partial e_0} X_{e_0}, \quad B_{p_0} = \prod_{e_0 \in \partial p_0} Z_{e_0}. \quad (1)$$

Here we use the symbols v_0 and p_0 to label vertex and plaquette operators. X_{e_0} and Z_{e_0} represent Pauli operators acting on qubit e_0 (we call e_0 as “edge”). A_{v_0} is the product of four Pauli X operators around vertex v_0 and B_{p_0} is the product of four Pauli Z operators around plaquette p_0 . We assume the lattice contains N vertices, N plaquettes and $2N$ edges. $2N$ physical qubits are put on each edge of the lattice. Its four-dimensional code subspace is stabilized by all A_{v_0} ’s and B_{p_0} ’s which is achieved through projective measurement of these stabilizers. Specifically, we start with the logical $++$ state by project all the B_{p_0} ’s to $+1$ for a product state of physical qubits $\bigotimes_{e_0} |+\rangle_{e_0}$:

$$|++\rangle = \prod_{p_0} \frac{I + B_{p_0}}{2} \bigotimes_{e_0} |+\rangle_{e_0} \quad (2)$$

and other logical bases are obtained by applying logical Pauli Z operators, $|--\rangle = Z_{l_1} |++\rangle$, $|+-\rangle = Z_{l_2} |++\rangle$ and $| - - \rangle = Z_{l_1} Z_{l_2} |++\rangle$. Here l_1 and l_2 denote non-contractible loops on the periodic lattice. Logical Pauli Z operators Z_{l_1} and Z_{l_2} are product of Z ’s along these non-contractible loops. Correspondingly there are also logical Pauli X operators $X_{l_1}^*$

and $X_{l_2^*}$, which are defined as X 's along non-contractible loops of the dual lattice, as in Fig. 1(a). The code subspace \mathcal{C} is spanned by these four logical bases.

III. MODEL FOR IMPERFECT MEASUREMENT

Experimentally, the stabilizer measurements are implemented using a multi-qubit unitary operation on a combined qubit set consisting of four data qubits and an ancilla qubit, followed by an ancilla qubit measurement [28, 45], also refer to Fig. 1(c). The correct projective measurements of stabilizers can only be achieved through ideal unitary operations. However, the multi-qubit operation in principle cannot avoid the miscalibration in the experimental setups and results in imperfect measurement [42]. Here we consider a simplified imperfect measurement model [43] [refer to Fig. 1(d)]: (1) Prepare the ancilla qubit in $|+\rangle$ state for each plaquette p_0 ; (2) apply a joint time evolution involving each ancilla and its four neighboring data qubits $\exp[-itZ_{p_0} \otimes B_{p_0}]$ where Z_{p_0} is the Pauli Z acting on ancilla at p_0 ; (3) perform projective measurement on ancilla in Y basis. Then equivalently we get a non-unitary evolution acting on the data qubits

$$M_{\{s_{p_0}\}} = \frac{1}{(\sqrt{2 \cosh \beta})^N} \exp \left[\frac{1}{2} \beta \sum_{p_0} s_{p_0} B_{p_0} \right]. \quad (3)$$

up to an irrelevant global phase factor. Here $\tanh(\beta/2) = \tan t$, and $s_{p_0} = \pm 1$ is the measurement outcome of ancilla qubit at p_0 . We use $\{s_{p_0}\}$ to denote the configuration of ancilla measurement outcomes, which appears with probability $\text{tr}(M_{\{s_{p_0}\}} \rho M_{\{s_{p_0}\}}^\dagger)$ for a given initial state ρ of data qubits. The error model [43] only considers the miscalibration of the evolution time t . For convenience, we restrict t to the region $0 \leq t \leq \pi/4$. When $t = \pi/4$, we have $\beta \rightarrow +\infty$ in Eq. (3) and recover the correct projective measurement $M_{\{s_{p_0}\}} \propto \prod_{p_0} (I + s_{p_0} B_{p_0})/2$. For $t \leq \pi/4$ the parameter β is finite, and $M_{\{s_{p_0}\}}$ will no longer be a stabilizer projection. This situation is referred to as weak measurement in Ref. [43]. Generally, β measures how 'strong' the measurement is, or equivalently how close is our imperfect measurement to the ideal projective measurement. So we call it the measurement strength. Moreover, it is easy to verify that the $E_{\{s_{p_0}\}} = M_{\{s_{p_0}\}}^\dagger M_{\{s_{p_0}\}}$ operators form a set of positive operator-valued measurement (POVM). A similar construction can also be applied to A_v stabilizers.

The above model is a rather simplified one which is easier to study analytically, but it can capture the fundamental influence of imperfect stabilizer measurement on QEC. We will show that even such a simplified imperfect measurement model will drastically affect QEC. A more realistic imperfect measurement model will in general has a worse performance, see the discussion of Eq. (27).

Experimentally while preparing the initial logical state through stabilizer measurement as in Eq. (2), it might suffer from imperfect measurement. In our model, the imperfect

initial logical $++$ state is considered as

$$|\widetilde{++}\rangle = \frac{M_{\{+\}} \otimes_{e_0} |+\rangle_{e_0}}{\sqrt{\otimes_{e_0} \langle +|_{e_0} M_{\{+\}}^\dagger M_{\{+\}} \otimes_{e_0} |+\rangle_{e_0}}}, \quad (4)$$

where $M_{\{+\}}$ denotes the imperfect measurement operator (3) when all the ancilla measurement outcomes s_{p_0} are set to $+1$. In the real world if the measurement outcomes contain an even number of -1 's, we can redefine the corresponding stabilizers with a minus sign, and the following discussion still works. If there are an odd number of -1 's, we drop it by post-selection. Actually, the odd parity results arise with a small probability for large enough β (refer to Sec. SI of supplemental information (SI) [46] for more details). Following the method in Ref. [43, 47] one can argue that these states possess only short-range entanglement by mapping them to a 2-d \mathbb{Z}_2 lattice gauge theory. But here in this work, we are mainly concerned about the influence on QEC and error threshold properties similar to Ref. [27]. We define the other three logical states by applying logical Z operators in analogy to experimental setups, $|\widetilde{-+}\rangle = Z_{l_1} |\widetilde{++}\rangle$, $|\widetilde{+-}\rangle = Z_{l_2} |\widetilde{++}\rangle$ and $|\widetilde{--}\rangle = Z_{l_1} Z_{l_2} |\widetilde{++}\rangle$. Unlike the projective measurement case, these logical states now depend on the choice of logical operators about where they locate on the physical lattice. However, due to the simpleness of our model, we can still verify that they are orthogonal to each other (refer to Sec. SI of SI [46]). We define the code subspace under imperfect measurement $\tilde{\mathcal{C}}(\beta)$ as the space spanned by these four logical states. Note that it depends on the measurement strength β during preparation. Here we mention that unlike projective measurement the image of $M_{\{s_{p_0}\}}$ acting on the whole Hilbert space is not a four-dimensional subspace but again the whole Hilbert space. That is why we cannot simply define code subspace as the image of $M_{\{s_{p_0}\}}$.

IV. STATISTICAL MECHANICAL MAPPING

Now we discuss the QEC property under imperfect measurement on the subspace $\tilde{\mathcal{C}}$ as the code space. Normally for toric code, the Pauli errors are detected by syndrome measurement. However, the syndrome measurement also suffers from imperfection resulting in faulty outcomes. Therefore, in order to distinguish measurement errors from Pauli errors, the standard procedure is to perform multi rounds of syndrome measurements and take into account the obtained entire error history while decoding [27]. Note that Ref. [27] only considered the stochastic (i.e. classical probabilistic) errors of the ancilla measurement, but we consider the coherent errors (i.e. quantum deviations) in the multi-qubit entanglement operations; and importantly, Ref. [27] assume a well-prepared initial state from the perfect code space, but we consider imperfect entanglement operations which affect both the initial state preparation and the error detection. We model the QEC procedure as follows (for convenience we consider only Pauli X errors):

- (1) Start with an arbitrary state $|\tilde{\Psi}\rangle \in \tilde{\mathcal{C}}(\beta_0)$, where we as-

sume the imperfect measurement strength while preparing the initial state is β_0 .

- (2) Probabilistic Pauli X error acts at each integer valued time t . The X error at each physical qubit on each time slice occurs independently with probability $q \in [0, 1/2]$.
- (3) Perform a round of syndrome measurement for each time interval between t and $t + 1$. The syndrome measurements are assumed to still suffer from imperfect measurement. So given a configuration of syndrome measurement outcomes $\{s_{p_0}\}$ for a single round, it leads to the action of $M_{\{s_{p_0}\}}$ operator on the current quantum state. Here we set the strength of syndrome measurements to be β in order to distinguish them from initial state preparation.
- (4) At the end of the QEC procedure, we decode and apply the Pauli X correction operator to the final state.

Before going any further, we mention that our relatively simple model ensures that the imperfection of measurement only affects stabilizer bits but does not disturb logical information, since $M_{\{s_{p_0}\}}$ commutes with logical operators.

Specifically, Notice that we can take the product of the eigenstates of $N - 1$ B_{p_0} operators, $N - 1$ A_{v_0} operators, and 2 logical operators $X_{l_1}^*$ and $X_{l_2}^*$ to form a complete basis of the whole Hilbert space of physical qubits. Under this basis, any state $|\tilde{\Psi}\rangle$ in the code space $\tilde{\mathcal{C}}$ can be expanded under the stabilizer basis to achieve the form (refer to Sec. SI of SI [46]):

$$|\tilde{\Psi}\rangle \propto \exp\left(\frac{\beta}{2} \prod'_{p_0} B_{p_0}\right) \bigotimes'_{p_0} \left[\sum_{b_{p_0}=\pm} \exp\left(\frac{\beta}{2} b_{p_0}\right) |B_{p_0} = b_{p_0}\rangle \right] \bigotimes'_{v_0} |A_{v_0} = +\rangle \bigotimes |L\rangle. \quad (5)$$

Here $|L\rangle$ stands for the logical information associated with the space defined by logical operators (Fig. 1(a)). Here we remark that the above tensor product at the r.h.s. is a mathematical structure using a non-local basis. Physically the logical information is still stored in a non-local manner for large β_0 . With this structure, it is clear that applying more rounds of imperfect measurement Eq. (3) on this state will not change the logical information $|L\rangle$.

So, if the Pauli X errors and the final correction operator compose a contractible loop (that can be factorized into B_{p_0} stabilizers and causes only trivial effect), we can verify that the logical information, i.e. $|L\rangle$ shown in Eq.(5), will still be preserved. We refer to this case as the success of QEC, in sharp contrast to the situation where we finally obtain a non-contractible loop and result in a logical error. Note that this condition for successful QEC is similar to the one in Ref. [27] while they only considered the probabilistic ancilla measurement error.

The above QEC procedure could be diagrammatically represented on a 3-d cubic lattice in order to decode as in Fig.

1(b). For convenience, we assume that the QEC starts at $t = -\infty$ and ends at $t = +\infty$, such that the 3-d corresponding spacetime lattice has infinite boundary condition at time direction. We use timelike and spacelike dual strings to represent measurement errors, i.e. faulty syndromes caused by imperfection of sequential measurements, and Pauli errors respectively. The error strings (including both measurement and Pauli parts) and syndrome strings (marked with -1 ancilla outcomes) together compose closed strings which have no endpoints (or end at infinity). The task of the decoder is to identify both measurement and Pauli errors. In order to do so, the decoder should select a configuration of strings (decoding strings) connecting the endpoints of syndrome strings. The timelike (spacelike) parts of the decoding strings represent the measurement (Pauli) error identified by the decoder. QEC succeeds if and only if the decoding strings are topologically equivalent to the real error strings (form contractible loops). So given an error syndrome, the optimal decoder algorithm (maximum likelihood decoder [31]) should select the topological equivalent class of error strings with the largest probability.

Our main result is that we mapped this QEC scenario to an SM model. We denote the vertex, edge and plaquette of the 3-d spacetime lattice as v , e and p . Specifically, the spacelike edges and plaquettes will be labeled with a subscript s , such as e_s and p_s . The timelike ones will be labeled with t , such as e_t and p_t . We assign a variable $\eta_p = \pm 1$ to each plaquette p to represent the error configuration, e.g. $\eta_p = -1$ for where the measurement or Pauli error presents and $+1$ otherwise. Then the probability of a given error configuration $\{\eta_p\}$ will be

$$P(\{\eta_p\}) = \frac{\sum_{\{\sigma_{e_0}\}} \exp\left[\beta_0 \sum_{p_0} b_{p_0} + \beta \sum_{p_s} b_{\Pi(p_s)} \eta_{p_s} + K \sum_{p_t} \eta_{p_t}\right]}{4^N (\cosh^N \beta_0 + \sinh^N \beta_0) (2 \cosh \beta)^{NT} (2 \cosh K)^{2NT}}, \quad (6)$$

where

$$b_{p_0} = \prod_{e_0 \in \partial p_0} \sigma_{e_0}, \quad K = -\frac{1}{2} \log \frac{q}{1-q}. \quad (7)$$

Here σ_{e_0} is a classical \mathbb{Z}_2 spin-like variable assigned to each edge e_0 of the 2-d physical lattice. b_{p_0} is the product of four neighbouring σ_{e_0} 's around the plaquette p_0 , which has the similar form to a \mathbb{Z}_2 gauge interaction term [48]. The T in this expression representing the total number of time steps will eventually be taken to $+\infty$. The summation $\sum_{\{\sigma_{e_0}\}}$ runs over all $\{\sigma_{e_0}\}$ configurations. The detail of derivation for this expression can be found in Sec. SII of SI [46]. Here we provide a brief explanation. First notice that given a quantum state ρ , the probability of POVM outcome is $\text{tr}(E_{\{s_{p_0}\}} \rho)$. We may construct a probability of syndrome measurement outcomes of all time steps and space locations conditioned on a fixed Pauli error configuration, which is expressed as

$$P(\{s_{p_0}(t)\}|\{\eta_{e_0}(t)\}) = \|\prod_t M_{\{s_{p_0}(t)\}} X_{\{\eta_{e_0}(t)\}} |\tilde{\Psi}\rangle\|^2 \quad (8)$$

for an arbitrary initial state $|\tilde{\Psi}\rangle$ in the imperfect code space $\tilde{\mathcal{C}}(\beta_0)$. Specifically, any initial state should be a superposition of imperfect logical states $|\tilde{\Psi}\rangle = \Psi_{++}|\widetilde{++}\rangle + \Psi_{+-}|\widetilde{+-}\rangle + \Psi_{-+}|\widetilde{-+}\rangle + \Psi_{--}|\widetilde{--}\rangle$ and we assume it to be normalized. Here $\{s_{p_0}(t)\}$ and $\{\eta_{e_0}(t)\}$ denotes the syndrome configuration and Pauli error configuration at time t . Note that a pair (p_0, t) yields a corresponding spacelike plaquette p_s and a pair (e_0, t) yields a corresponding timelike plaquette p_t . $X_{\{\eta_{e_0}(t)\}}$ is the total Pauli error operator at time t , and has the form

$$X_{\{\eta_{e_0}(t)\}} = \prod_{e_0} (\delta_{\eta_{e_0}(t), +1} I + \delta_{\eta_{e_0}(t), -1} X_{e_0}). \quad (9)$$

We can check that Eq. (8) is a well-defined joint probability and it matches the physical POVM probability at each time step, which ensures the effectiveness of SM mapping (see Sec. SII of SI [46]). A explicit calculation of Eq. (8) yields that

$$P(\{s_{p_0}(t)\}|\{\eta_{e_0}(t)\}) = \frac{1}{4^N (\cosh^N \beta_0 + \sinh^N \beta_0) (2 \cosh \beta)^{NT}} \times \sum_{\{\sigma_{e_0}\}} \exp \left[\sum_{p_0} b_{p_0} \left(\beta_0 + \beta \sum_t s_{p_0}(t) \prod_{k \leq t} \prod_{e_0 \in \partial p_0} \eta_{e_0}(k) \right) \right]. \quad (10)$$

Note that Eq. (10) does not depend on the choice of $|\tilde{\Psi}\rangle$. The σ_{e_0} variables are obtained by expanding the quantum states under the computational basis (a technic developed in Ref. [43, 47] dealing with post-measurement states), and the term $\prod_{e_0 \in \partial p_0} \eta_{e_0}(k)$ marks the boundary of Pauli error strings at time k . Since the measurement error configuration can be inferred from the boundary of Pauli error strings and syndrome outcomes, its corresponding probability can be obtained by substituting syndrome variables with combinations of Pauli and measurement error variables

$$\eta_{p_0}(t) = s_{p_0}(t) \prod_{k \leq t} \prod_{e_0 \in \partial p_0} \eta_{e_0}(k). \quad (11)$$

After combining with Pauli error probability

$$P(\{\eta_{e_0}(t)\}) = \prod_{e_0, t} q^{\delta_{\eta_{e_0}(t), -1}} (1 - q)^{\delta_{\eta_{e_0}(t), +1}} = \prod_{e_0, t} \frac{\exp(K \eta_{e_0}(t))}{2 \cosh K}, \quad (12)$$

we arrive at a joint probability of total error configurations,

$$P(\{\eta_{p_0}(t)\}, \{\eta_{e_0}(t)\}) = \frac{P(\{\eta_{p_0}(t)\}|\{\eta_{e_0}(t)\})P(\{\eta_{e_0}(t)\})}{1} = \frac{1}{4^N (\cosh^N \beta_0 + \sinh^N \beta_0) (2 \cosh \beta)^{NT} (2 \cosh K)^{2NT}} \times \sum_{\{\sigma_{e_0}\}} \exp \left[K \sum_{e, t} \eta_{e_0}(t) + \sum_{p_0} b_{p_0} \left(\beta_0 + \beta \sum_t \eta_{p_0}(t) \right) \right], \quad (13)$$

which is exactly Eq. (6) after converting the notations to those of the 3-d lattice. Here, the fact $P(\{\eta_p\})$ can be derived as a

well-defined joint probability for each η_p is a consequence of the simpleness of our error model.

Then following the standard procedure described in Ref. [27, 29, 31], we computed the probability of the topological equivalent class of error configurations and it is proportional to the partition function of an SM model

$$P(\{[\eta_p]\}) \propto \mathcal{Z}(\{\eta_p\}) = \sum_{\{\sigma_{e_0}\}, \{\tau_e\}} \exp \left[\beta_0 \sum_{p_0} b_{p_0} + \beta \sum_{p_s} b_{\Pi(p_s)} \eta_{p_s} U_{p_s} + K \sum_{p_t} \eta_{p_t} U_{p_t} \right], \quad U_p = \prod_{e \in \partial p} \tau_e. \quad (14)$$

This SM model is a 3-d \mathbb{Z}_2 gauge theory defined on the space-time lattice coupled to a 2-d \mathbb{Z}_2 gauge theory defined on the physical lattice, see Fig. 2. Here $\tau_e = \pm 1$ is a spin variable defined on each edge e of the spacetime lattice. U_p is an ordinary \mathbb{Z}_2 gauge interaction term containing four τ_e operators, $[\{\eta_p\}]$ denotes the topological equivalent class represented by $\{\eta_p\}$, and η_p sets the sign of interaction term on each plaquette. The summation of $\{\tau_e\}$ configurations is the same as a summation over topologically equivalent error configurations up to a constant factor. Physically, those τ_e operators describe the fluctuation of error strings, since flipping τ_e operator is equivalent to deforming the error strings represented by $\{\eta_p\}$ (see detail discussions in Ref. [27, 29]). Therefore, the model acquires a local symmetry

$$\eta_p \rightarrow \eta_p \prod_{e \in \partial p} \nu_e, \quad \tau_e \rightarrow \tau_e \nu_e, \quad \nu_e = \pm 1, \quad (15)$$

which ensures that topologically equivalent error configurations yield the same partition function. In order to detect the error threshold, Eq. (6) should be considered as the quenched disorder probability of interaction configuration $\{\eta_p\}$. Then the phase transition point of τ_e spins in the disordered SM model should correspond to the error threshold of the QEC model [27, 29, 31]. The reason for this phase transition-error threshold correspondence is as follows. Recall that the optimal decoder algorithm will select the equivalent class (of error configuration) with the largest probability or the smallest free energy. Define the free energy cost of an arbitrary non-contractible loop configuration $l = \{\eta_p^l\}$ as

$$\Delta_l = - \sum_{\{\eta_p\}} P(\{\eta_p\}) \log \frac{\mathcal{Z}(\{\eta_p \cdot \eta_p^l\})}{\mathcal{Z}(\{\eta_p\})}. \quad (16)$$

In the ordered phase, Δ_l diverges if we take the thermodynamic limit along with a disorder average. This suggests that the probability of the correct equivalent class will be far larger than that of the wrong one differed by a non-contractible loop, since the probability of an equivalent class is proportional to the partition function. Thus the optimal decoder always succeeds. In the disordered phase, however, the finiteness of free energy cost signifies the failure of the optimal decoder. A detailed explanation can be found in Ref. [31] for the case with stochastic errors.

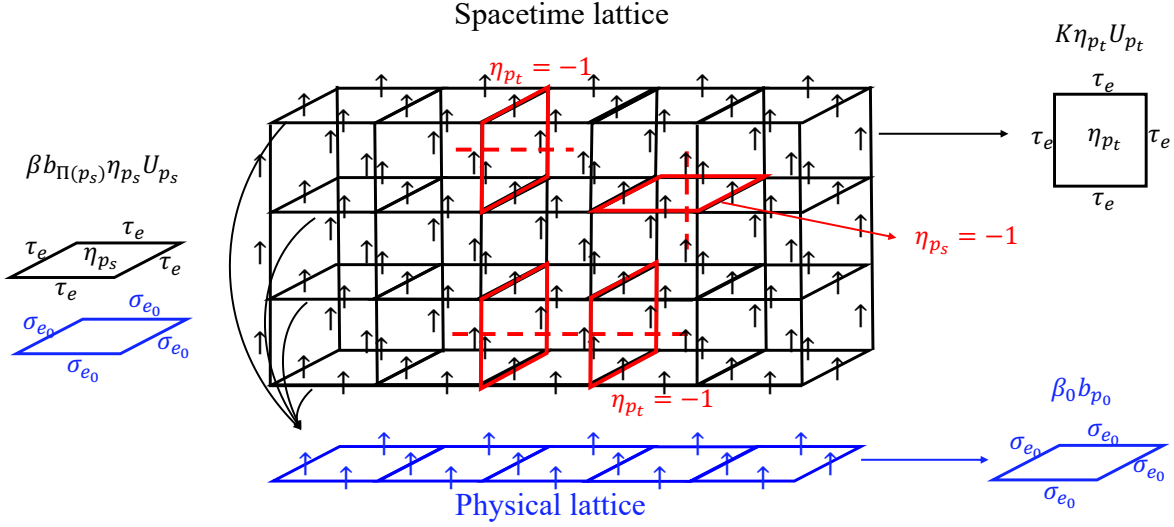


Figure 2. Illustration of the SM model we obtained in Eq. (14). The τ_e spins are defined on the edges of 3-d spacetime lattice and the σ_{e_0} spins lie on 2-d physical lattice. There are three types of interactions in this model as shown in this figure. $\beta_0 b_{p_0}$ is the gauge interaction term defined on the physical lattice. $K\eta_{p_t}U_{p_t}$ is the timelike gauge interaction on spacetime lattice. The $\beta b_{\Pi(p_s)}\eta_{p_s}U_{p_s}$ term couples the spacelike gauge interaction term U_{p_s} to the gauge interaction term $b_{\Pi(p_s)}$ on physical lattice. The η_p 's set the signs of gauge interactions on spacetime lattice and they mark the position of error strings during the QEC procedure in Fig. 1(b). For example, the flipped interaction $\eta_p = -1$ at plaquette p (red plaquette) corresponds to the presence of an error string at p (dashed red line). The $\{\eta_p\}$ configuration follows a disorder probability (6) that comes from the randomness of Pauli errors and in syndrome measurement. The τ_e spins are non-locally correlated at timelike direction since all spacelike plaquette interactions U_{p_s} along the same timelike arrow are all coupled to the same $b_{\Pi(p_s)}$. Meanwhile, the disorder probability (6) is also correlated at time direction. Physically this is due to the fact imperfection measurement operator will change the current quantum state, which in turn affects subsequent measurement results. It is evident from the expressions (14) and (6) that the non-local correlation results from finite β_0 , or in other words imperfect initial state preparation.

V. PHASE STRUCTURE OF THE STATISTICAL MECHANICAL MODEL

Here we provide some analytical results about the SM model and its phase structure. First, we notice that the SM model has a non-local correlation at time direction originates from imperfect initial state preparation, see Fig. 2. If we set β_0 to $+\infty$, then the initial state is well prepared and the code space $\tilde{\mathcal{C}}(\beta_0)$ becomes exactly the toric code subspace. The action of following syndrome measurement operators Eq. (3) on this space yields only a global phase factor and does not change the state itself. In this case, even though the measurement outcome can still be faulty, the probability of measurement error will now become uncorrelated. This reduces to a pure probabilistic measurement error model considered in Ref. [27]. At the SM model side, by taking β_0 to $+\infty$ we self-consistently arrive at the random plaquette gauge model (RPGM) derived also in Ref. [27].

In reality, the same faulty circuits that produce the imperfect syndrome measurements also provide the imperfect initial state preparations. In this situation, i.e. with finite β_0 , the non-local timelike correlation will lead to a different phase structure in stark contrast to RPGM. In the following paragraphs, we will explore this phase structure in detail. In order to detect the phase transition of τ_e spins, we consider the Wilson

loop

$$W_A = \prod_{p \in A} U_p = \prod_{e \in \partial A} \tau_e, \quad (17)$$

which serves as the order parameter for \mathbb{Z}_2 gauge theory. Different phases of the gauge theory can be distinguished based on the fact whether the Wilson loop confines or deconfines. Here A is a set of plaquettes representing a surface in space-time. The product of U_p 's on surface A equals the product of τ_e 's on ∂A , which is the boundary of surface A and forms a closed loop. In the conventional \mathbb{Z}_2 gauge theory [48] the scaling behavior of Wilson loop expectation values with respect to the loop size distinguishes between the confinement (disordered) phase and the deconfinement (ordered) phase. In the deconfinement phase, it decays exponentially with respect to the perimeter of the loop,

$$W_A \sim \exp(-\text{const} \times |\partial A|), \quad (18)$$

called perimeter law. Here we use $|\cdot|$ to denote the cardinal of a set (i.e. the number of the elements of a set). For example $|\partial A|$ is the number of edges contained in ∂A . On the other hand, in the confinement phase, the scaling behavior of Wilson loops obeys area law,

$$W_A \sim \exp(-\text{const} \times |A_{\min}|), \quad (19)$$

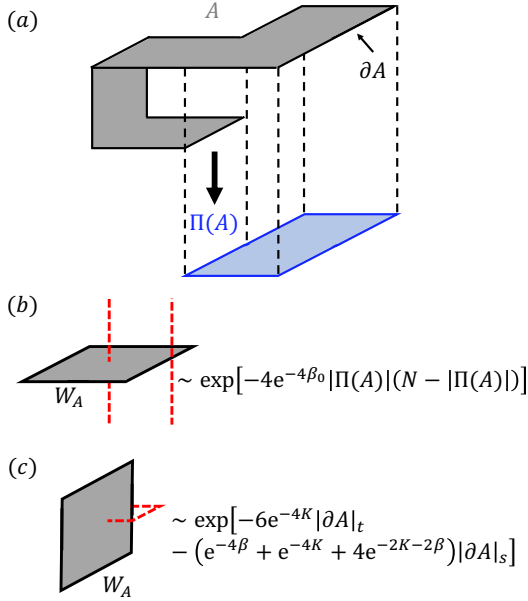


Figure 3. (a) Example of a Wilson loop. A is a surface in 3D spacetime (gray) and ∂A is its boundary (black), which is a closed loop. $\Pi(A)$ is the projection of surface A from 3D spacetime to 2D space mod \mathbb{Z}_2 . Specifically, under projection the timelike plaquettes are dropped, and an even number of spacelike plaquettes at the same space position also vanishes. The only remaining plaquettes are at the spatial locations that originally have odd numbers of spacelike plaquettes. In (b) and (c), the black lines represent Wilson loops and the red dashed lines are examples of topologically trivial error strings created by τ_e fluctuation. (b) A spacelike Wilson loop. In a large enough system it decays exponentially with respect to the area for any finite temperature. Note that Its scaling behavior written in the figure directly follows from Eq. (21) by constraining A to a pure spacelike region. For a large region A , the areal decay will be much faster than the perimetric decay, so the first term in Eq. (21) dominates. This behavior is contributed by the fluctuation of infinite long timelike error strings which are able to appear at any space position (see Sec. SIV of SI [46]). (c) A timelike Wilson loop. Its scaling behavior is obtained by constraining A to a pure timelike region in Eq. (21). Under a low temperature, it decays exponentially with respect to the perimeter. Note that both timelike edges and spacelike edges are contained in the boundary of a timelike region, determining the $|\partial A|_t$ term and $|\partial A|_s$ term respectively. This perimetric decay behavior is mainly contributed by local error loops near the Wilson loop (see Sec. SIV of SI [46]).

where A_{min} is the minimal surface enclosed by ∂A . Here we will study the expectation value of Wilson loops in our SM model.

First, note that our SM model satisfies a generalized version of Nishimori condition [49, 50], which means that the error rate parameters (β_0, β, K) in the quenched disorder probability in Eq. (6) are the same as those in the partition function in Eq. (14), respectively. Under this condition, by taking advantage of a local symmetry of the model (15), we find that (see

Sec. SIII of SI [46])

$$[\langle W_A \rangle] = [\langle W_A \rangle^2]. \quad (20)$$

Here $\langle \cdot \rangle$ denotes the ensemble average with respect to the model Eq. (14) under a specific interaction configuration. $[\cdot] = \sum_{\{\eta_p\}} P(\{\eta_p\}) (\cdot)$ represents the disorder average over interaction configurations with respect to the probability Eq. (6). The above equality suggests the absence of gauge glass phase [51] ($[\langle W_A \rangle]$ obeys area law Eq. (19) but $[\langle W_A \rangle^2]$ obeys perimeter law Eq. (18)) so that we only need to concern about the deconfinement-confinement phase transition of τ_e 's under Nishimori condition.

We then perform a low-temperature expansion [48] for $[\langle W_A \rangle]$. Here low temperature means that the parameters β_0, β and K are sufficiently large, corresponding to small enough physical error rates. We assume $e^{-\beta_0}, e^{-\beta}$ and e^{-K} are of the same order and expand $\log[\langle W_A \rangle]$ up to the first non-vanishing order $e^{-4\beta_0}$. We obtain the result (refer to Sec. SIV of SI [46] for more details)

$$\begin{aligned} [\langle W_A \rangle] &\simeq \exp[-4e^{-4\beta_0} |\Pi(A)| (N - |\Pi(A)|)] \\ &\quad - (e^{-4\beta} + e^{-4K} + 4e^{-2\beta-2K}) |\partial A|_s - 6e^{-4K} |\partial A|_t. \end{aligned} \quad (21)$$

Here Π is defined as projection from 3-d spacetime to 2-d space mod \mathbb{Z}_2 , illustrated in Fig. 3(a). $|\partial A|_s$ ($|\partial A|_t$) denotes the spacelike (timelike) edges e_s (e_t) contained in ∂A . The low temperature expansion is done by first expanding $P(\{\eta_p\})$ up to $e^{-4\beta_0}$. Then for each error configuration that appeared in the expansion, we compute the expectation value $\langle W_A \rangle$ up to the order we need. The perturbative evaluation of $\langle W_A \rangle$ is accomplished by identifying the ground state and then taking the lowest excited states into consideration. Each of these states yields a specific value of W_A . Putting all these things together, we obtain Eq. (21).

From this expression, we see that the expectation value of Wilson loops has an anisotropic scaling behavior. It deconfines at the timelike direction under low temperature but confines at the spacelike direction for any finite β_0 (Fig. 3). A pure timelike Wilson loop W_A which contains only timelike plaquettes is shown in Fig. 3(c). It deconfines and decays exponentially with respect to perimeter as in a conventional 3-d \mathbb{Z}_2 lattice gauge theory under low temperature. Meanwhile, a pure spacelike Wilson loop is shown in Fig. 3(b). For large enough system size N , its areal decay is faster than the perimetric decay, so the first term in Eq. (21) dominates and $[\langle W_A \rangle]$ confines as long as the temperature is finite. We notice that no matter how low the non-zero temperature is, the confinement is always maintained. Since a sufficiently high temperature should drive the system into a completely disordered phase, it will confine all Wilson loops. Specifically, we do not expect the deconfinement of spacelike Wilson loops at higher temperatures. Thus we conclude that spacelike Wilson loop confines at any finite temperature (or error rate). At a sufficiently high temperature (or error rate), we expect a phase transition that confines the timelike Wilson loop. We also noticed from Eq. (21) that this areal decay is a consequence of imperfect measurement during initial state preparation. Consistently, we find in our derivation that the area term results

from the non-local timelike correlation of disorder probability Eq. (6) and partition function Eq. (14) which also depends on β_0 as we discussed. In comparison, if the initial state is ideally prepared ($\beta_0 = +\infty$, corresponds to RPGM), the Wilson loops will acquire an isotropic scaling behavior, i.e. both the spacelike and timelike Wilson loops will exhibit perimeteric decay at the low-temperature phase and areal decay at the high-temperature phase [27].

Here we also remark that the low-temperature expansion result shown in Eq. (21) is valid for any finite system size N and region A , as long as the temperature (physical error rate) is sufficiently low. The subtlety is that we cannot directly take the thermodynamic limit $N \rightarrow +\infty$ in Eq. (21) because of the factor N contained in the leading order. Actually, the appearance of area term $|\Pi(A)|(N - |\Pi(A)|)$ in Eq. (21) is a natural result because our space manifold is a closed surface (due to the periodic boundary condition), thus $\Pi(A)$ and its complement on 2-d space yield the same boundary, and should be symmetric in an expression containing $|\Pi(A)|$. However under the thermodynamic limit, the phase structure of the SM model should not depend on this boundary condition, and we expect that the area law is still obeyed by spacelike Wilson loops in the low-temperature phase. A brief discussion about the analogy to the exactly solvable 2-d \mathbb{Z}_2 lattice gauge theory can be found in Sec. SIV of SI [46].

VI. IMPACT ON QUANTUM ERROR CORRECTION

In the previous sections, we mapped our QEC model under imperfect measurement and Pauli error to an SM model and studied the phase structure of the SM model. The question is what these results imply about for QEC performance and threshold theorem. Here we provide an interpretation of these results.

First of all, knowing that there exists a confinement transition point of timelike Wilson loops in the limit $T \rightarrow +\infty$ and $N \rightarrow +\infty$, we want to ask how it relates to the logical error rate and error threshold. In fact, we find that the logical error rate is suppressed at the low-temperature phase. Note that the fluctuation of topologically trivial error strings is described by the fluctuation of τ_e 's (refer to the discussion of Eq. (15)). Each fluctuated spin configuration will contribute to the expectation value of Wilson loop. So the behaviors of Wilson loops reflect features of error string fluctuations. In our derivation of low-temperature expansion (also see Sec. SIV of SI [46]), we find that: 1) the areally decaying behavior of spacelike Wilson loop results from non-local timelike error strings like in Fig. 3(b); 2) the non-local timelike strings and other local error loops appear in a relatively independent manner at sufficiently low temperatures. Therefore, those local error loops are compressed and are unlikely to stretch to arbitrarily large. Specifically, the fluctuating error strings cannot extend arbitrarily long in space direction. Since the non-contractible loops can only wind around spacelike directions, we still expect their free energy cost, i.e. Δ_l shown in Eq. (16), to diverge, hence the logical error rate approaches zero. Increasing the temperature, there should be a transition

point where spacelike error strings become extending along the whole system and Δ_l becomes finite, and thus the probability of logical error acquires a finite value. This transition point of Δ_l should be exactly the confinement point of timelike Wilson loops. Since the confinement transition point of timelike Wilson loops separates different behavior of logical error rate in the limit $T \rightarrow +\infty$ and $N \rightarrow +\infty$, it is appealing to identify this transition point as the threshold, which we refer to as theoretical threshold. However, this threshold, which we will find later, does not capture the correctability of measurement error.

We want to emphasize that, only for the infinite-time syndrome scenario, the theoretical threshold in our model can faithfully determines the success of QEC as we discussed in the last paragraph. However, due to the unidentifiable even below the theoretical threshold, the decoding procedure fails while considering a finite time syndrome information. In the infinite-time case, the decoder takes an infinite error history to enhance the power of QEC. But in reality, we can only store finite error history, where the areal decay of spacelike Wilson loops drastically affects the QEC. Roughly speaking, in the real world the decoder must be applied to a finite time interval of size T . Then problems arise while trying to correct measurement errors in the finite-time scenario. Recall that the areal decay of spacelike Wilson loops signifies error strings can stretch infinitely along the timelike direction. This suggests that measurement errors can easily extend from the beginning to the end and become generally undistinguishable from Pauli errors. For example, the true syndrome of a single Pauli error string will be two non-local timelike strings starting from its boundary points. Meanwhile, this syndrome can also be created by non-local measurement errors, which could occur with a probability close to the one of the Pauli string and cannot be suppressed by large T . The consequence is that the decoder might mix up these two situations with a finite probability and leave this Pauli error uncorrected (the correction operator determined by the decoder will not be containing this Pauli string). From this example, we infer that due to the presence of non-local measurement errors, there will be Pauli errors remaining uncorrected at the end of the QEC procedure, which means that the combined strings of the Pauli error operator and correction operator will still have an amount of open ends. If these open-ended strings anticommute with logical Z operators, it will damage the logical information $|L\rangle$ (refer to the discussion of Eq. (5)). This situation does not have much difference from the case when only a single round of syndrome measurement is performed ($T = 1$), since the probabilities of non-local measurement errors do not depend on T .

We conclude that for a large system size N , the ability to identify measurement errors cannot be enhanced by increasing the number of syndrome measurement rounds, even below the theoretical threshold. This is in stark contrast to the case with only stochastic errors [27], where the perimeter law for both the spacelike and timelike Wilson loops guarantees the achievement of an effective error correction with a finite error history whenever the error rate is below the theoretical threshold. In our case, the inability to correct measurement errors is

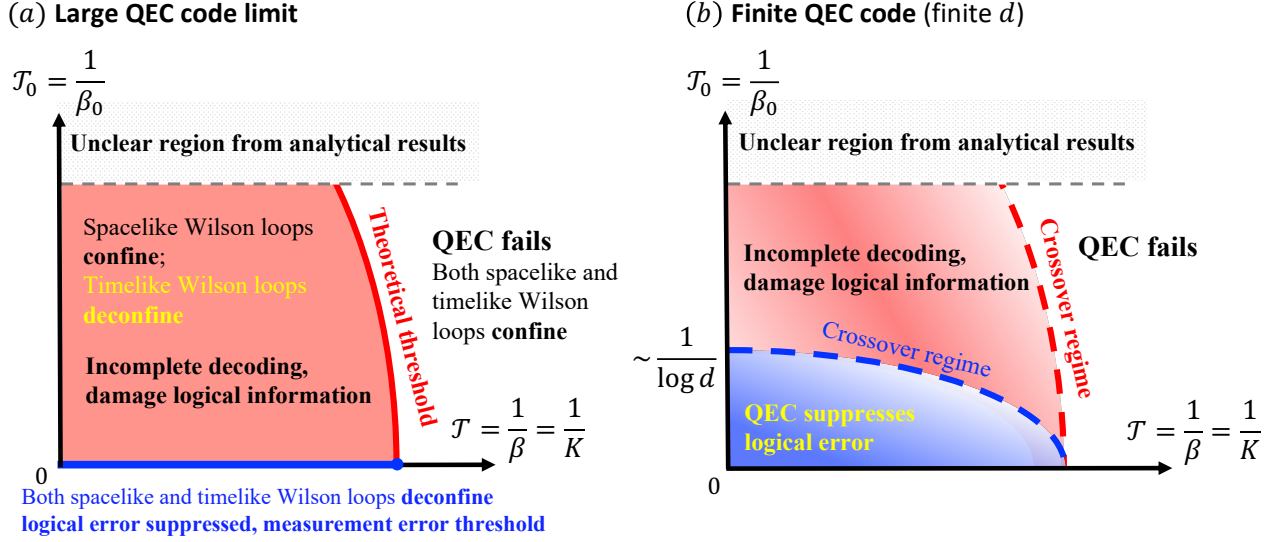


Figure 4. (a) Our estimation of the phase structure in the thermodynamic limit $T \rightarrow +\infty$ and $N \rightarrow +\infty$ while setting $\mathcal{T} = 1/\beta = 1/K$ and $T_0 = 1/\beta_0$. Above the theoretical threshold (red line) QEC fails due to non-contractible logical Pauli errors. Below the theoretical threshold and above the measurement error threshold (blue line), non-contractible logical Pauli errors are suppressed. However, measurement errors are still unidentifiable through decoding a finite error history and will be confounded with Pauli errors. Note that the \mathcal{T} axis where $T_0 = 0$ represents the RPGM. While the theoretical threshold intersect with the \mathcal{T} axis at the common RPGM phase transition point [27], we are not sure yet whether it intersect with the T_0 axis. Some details at higher temperatures still requires further investigation. For completeness, we note that if $K \rightarrow +\infty$, the QEC protocol trivially succeeds as there will be no Pauli errors. On the other hand, in the scenario where $\beta \rightarrow +\infty$ but K and β_0 are finite, the non-local measurement errors are still present and cannot be decoded when confounded with Pauli errors. (b) The phase diagram while fixing a finite code distance d . The phase transitions (thresholds) in Fig. 4(a) are smoothed into crossovers due to finite-size effect. Especially, the measurement error threshold becomes a finite-temperature crossover (blue dashed line), leading to a parameter region with a finite area (light blue region) that effectively suppresses logical errors. The parameters in this region should satisfy either Eq. (22) or Eq. (23) such that the non-local measurement errors will not be a problem. Specifically, the crossover condition $T_0 \sim 1/\log d$ near the T_0 axis is derived from Eq. (22) (However, Eq. (22) or Eq. (23) are only approximate expressions valid in the low-temperature limit. The precise value of this crossover still requires further investigation.). Increasing d , this region becomes smaller and smaller and eventually sticks to the \mathcal{T} axis. Above the crossover regime of measurement threshold in the light red region, the effect of non-local measurement errors on the QEC becomes non-negligible. As for the SM model side, the blue crossover detects the confinement of spacelike Wilson loops while the red crossover detects the confinement of timelike Wilson loops.

caused by the finite value of β_0 , i.e. the imperfection of initial state preparation; so we refer to $\beta_0 = +\infty$ as the measurement error threshold of our error model. Setting $\beta_0 = 1/T_0$ and $\beta = K = 1/\mathcal{T}$, a sketch of the phase diagram is shown in Fig. 4(a). In addition, an overall comparison of our error model and the model in Ref. [27] can be found in Tab. I.

As we have mentioned in the above paragraphs, the measurement errors are unidentifiable even at low temperatures, in the sense that the multi-round syndrome measurement protocol will not be better than a single-round one, i.e. $T = 1$ or a 2D decoder. So one might ask how the QEC behaves when $T = 1$. Suppose the QEC initial state is the imperfect logical 00 state $|\tilde{\Psi}\rangle = |00\rangle = (|++\rangle + |+-\rangle + |-+\rangle + |--\rangle)/2$, we estimate the impact of measurement errors on the logical fidelity, that is the fidelity between the final state and the initial state. Consider the scenario where the temperature is low and the system is of considerable size. In accordance with the preceding discourse, A Pauli error on a single physical qubit will be confounded with measurement errors having the same syndrome by the decoder. Consequently, the Pauli error will

remain uncorrected. If the uncorrected Pauli error intersects with a logical Pauli Z operator, it acts as a logical error on the logical information $|L\rangle$ (refer to Eq. (5)), leading to a logical fidelity ~ 0 . But if the Pauli error locates elsewhere on the lattice, one may check that the effects of the Pauli error and the measurement operator with the same syndrome complement each other and lead to a fidelity ~ 1 , since they both flip the same stabilizer bits in Eq. (5) but do not affect the logical information $|L\rangle$. Average all error configurations, since the number of configurations that a Pauli error intersects with logical Z is proportional to $d = \sqrt{N}$, we anticipate that the logical fidelity behaves as $1 - \text{const} \times d$. The logical fidelity is suppressed by a large distance, which is a signal that the QEC system is above the ture threshold (measurement error threshold in our work). Here the constant depends on the physical error rates β_0 , β and K but does not depend on the distance d , and it should drop to 0 when the initial state is ideal, $\beta_0 \rightarrow +\infty$.

In contrast, we compare it with the $T = 1$ case of Ref. [27], the 2D decoder suffering from stochastic measurement

	Our case	The case in Ref. [20]
Noise properties	1) coherent errors on entanglement gates of stabilizer measurement circuit (imperfect measurement), 2) stochastic Pauli errors on physical qubits	1) stochastic measurement errors of stabilizer measurement outcomes, 2) stochastic Pauli errors on physical qubits
Initial state	Affected by imperfect measurement during preparation (characterized by β_0)	Ideal toric code state
Error correction protocol	Multi-round syndrome measurement (number of rounds: T) and maximum likelihood decoder	
SM mapping	3-dimensional \mathbb{Z}_2 gauge model coupled to a 2-dimensional \mathbb{Z}_2 gauge model (Eq. (7)) with quenched disorder (Eq. (5))	3-dimensional RPGM under Nishimori condition
Phase structure of SM model	When $\beta_0 \rightarrow +\infty$ (ideal initial state), the SM model reduces to RPGM. For finite β_0 (imperfect initial state), in the low-temperature phase (below theoretical threshold) timelike Wilson loops deconfine but spacelike Wilson loops confine; in the high-temperature phase (above theoretical threshold) all Wilson loops confine.	In the low-temperature phase (below theoretical threshold) all Wilson loops deconfine; in the high-temperature phase (above theoretical threshold) all Wilson loops confine.
Error correction performance	When $\beta_0 \rightarrow +\infty$ (ideal initial state), it is equivalent to the model in Ref. [20]. For finite β_0 (imperfect initial state), in the low-temperature phase (below theoretical threshold) there are still unidentifiable measurement errors that damage QEC performance, no matter how large T is; in the high-temperature phase (above theoretical threshold) QEC fails due to logical errors (non-contractible error loops).	In the low-temperature phase (below theoretical threshold), the probability of QEC success can be enlarged by increasing N and T (note that the QEC always fails while $T = 1$ but logical errors can be effectively suppressed while $T \gg \sqrt{N}$); in the high-temperature phase (above theoretical threshold) QEC fails.

Table I. Comparison between our case and the case with the stochastic measurement error model [27]. Note that although the measurement noises of the two models are different at the physical level, their error correction properties and corresponding SM models will become equivalent when we set the initial state in our model to be ideal ($\beta_0 \rightarrow +\infty$).

errors. The decoder in this case also mixes up a Pauli error with probabilistic measurement errors, but their effects do not complement each other, since the probabilistic measurement error is just noise on the classical readouts and does not affect the quantum state. Consequently the logical fidelity scales as $1 - \text{const} \times d^2$, where the constant depends on the probability of Pauli and measurement errors. This logical fidelity is also above the threshold. Surprisingly, it is worse than the one of our model. However, the logical fidelity under stochastic errors can be improved by increasing T and arrives at an effective QEC when $T \gg d$ [27], which is not possible in our model.

One might argue that although the non-local measurement errors suppress logical fidelity, the correction of other local errors might lead to other terms that increase with d and compete with non-local measurement errors. However, the non-local measurement error suppression should be the leading order contribution in the low-temperature limit. Moreover, if the system lies above the blue crossover in the light red region in Fig. 4(b), the effect of non-local measurement errors overweighs other local errors. Thus we believe that the non-local measurement error suppression could overweight other terms in that region. Nonetheless, these statements are not rigorous proofs and require further studies.

For a small code with limited system size N , we infer from Eq. (21) that the above problem might be circumvented with

the limit

$$d \ll e^{\beta_0}, \quad (22)$$

or

$$d \ll [e^{4\beta_0}(e^{-4\beta} + e^{-4K} + 4e^{-2\beta-2K})]^{1/3}. \quad (23)$$

Here d is the code distance and $N = d^2$. The first bound is derived by assuming the areal term in Eq. (21) is negligible

$$e^{-4\beta_0} |\Pi(A)| (d^2 - |\Pi(A)|) \ll 1, \quad (24)$$

for all spacelike Wilson loops A . The l.h.s. maximizes when A is half the size of the spatial lattice $|\Pi(A)| = d^2/2$. Substitute $|\Pi(A)| = d^2/2$ into the above expression, we obtain Eq. (22) ignoring a constant factor. Physically, Eq. (22) is interpreted as the impact of measurement error itself on the system is ignorable. The second bound is derived by considering when the perimetric decay will be faster than the areal decay in Eq. (21) for a spacelike Wilson loop,

$$\begin{aligned} & e^{-4\beta_0} |\Pi(A)| (d^2 - |\Pi(A)|) \\ & \ll (e^{-4\beta} + e^{-4K} + 4e^{-2\beta-2K}) |\partial A|_s. \end{aligned} \quad (25)$$

Still we require A to be half of the spatial lattice, $|\Pi(A)| \sim d^2$ and $|\partial A|_s \sim d$. Thus we obtain Eq. (23). Physically, Eq.

(23) is interpreted as the influence of non-local error strings is not significant compared to other local error strings. If either of these two bounds is satisfied, we anticipate that the ability of our QEC procedure to detect measurement errors will be similar to that of Ref. [27]. To satisfy either Eq. (22) or Eq. (23), the imperfection of initial state preparation must be negligible or much smaller than the syndrome measurement imperfection and Pauli error rate. Even then the code distance is still upper bounded if we fix the error parameters β_0 , β and K . Usually, when performing QEC, we anticipate increasing code distance to suppress the logical error rate [28]. However, for the important error problem considered here, Eq. (22) and Eq. (23) form bounds that prevent the code from scaling up. Equivalently if we fix d and vary the error parameters, we obtain the phase diagram in Fig. 4(b). It is noteworthy that the region enabling pragmatic error correction only experiences a gradual reduction as increasing the code distance, i.e. $\sim 1/\log d$, which is not excessively frustrating.

VII. DISCUSSION

In this work, we discuss the imperfect measurement problem based on the circuit shown in Fig. 1(d) (e.g. for B_{p_0}), which allows us to conduct an analytic study. In fact, the circuit shown in Fig. 1(c), which contains only two-qubit gates rather than a five-qubit evolution in our simple model, is more realistic. Ref. [42] discussed an imperfect measurement model which mimics the behavior of superconducting quantum computation systems. The $CNOT$ gate is divided into a CZ gate and two Hadamard gates, $CNOT = H(CZ)H$ where H is the Hadamard gate acting on the target qubit (ancilla qubit in our setup). Each CZ gate is implemented by a time evolution

$$U = \exp \left[-i \frac{t}{4} (s^z \otimes \sigma_i^z - s^z \otimes I - I \otimes \sigma_i^z + I \otimes I) \right] \quad (26)$$

Here s labels the ancilla qubit and σ_i , $i = 1, 2, 3, 4$ labels the four data qubits. It recovers the CZ gate when $t = \pi$. Assume the final ancilla measurement has an outcome $s = \pm 1$, the corresponding action on data qubits is

$$\begin{aligned} M_s = \langle s | H \exp \left[-i \frac{t}{4} \sum_i (s^z \otimes \sigma_i^z - s^z \otimes I - I \otimes \sigma_i^z + I \otimes I) \right] H | 0 \rangle = \frac{1}{2} \left(1 + se^{-i2t} \cos^4 \frac{t}{2} + se^{-i2t} \sin^4 \frac{t}{2} B_{p_0} \right) \\ \times \left(1 - \frac{ise^{i2t} \sin \frac{t}{2} \cos^3 \frac{t}{2} + i \sin \frac{t}{2} \cos^7 \frac{t}{2} + i \sin^7 \frac{t}{2} \cos \frac{t}{2}}{(se^{i2t} + \cos^4 \frac{t}{2})^2 - \sin^8 \frac{t}{2}} \sum_i \sigma_i^z - \frac{\sin^2 \frac{t}{2} \cos^2 \frac{t}{2}}{se^{i2t} + \cos^4 \frac{t}{2} + \sin^4 \frac{t}{2}} \sum_{i < j} \sigma_i^z \sigma_j^z \right. \\ \left. + \frac{ise^{i2t} \sin^3 \frac{t}{2} \cos \frac{t}{2} + i \sin^3 \frac{t}{2} \cos^5 \frac{t}{2} + i \sin^5 \frac{t}{2} \cos^3 \frac{t}{2}}{(se^{i2t} + \cos^4 \frac{t}{2})^2 - \sin^8 \frac{t}{2}} \sum_{i < j < k} \sigma_i^z \sigma_j^z \sigma_k^z \right). \end{aligned} \quad (27)$$

When $t = \pi$, one may check that the above expression reduces to the correct projection $(I + sB_{p_0})/2$. When $t \neq \pi$, M_s stands for an imperfect measurement operator. We notice that in its expression the first factor $1 + se^{-i2t} \cos^4(t/2) + se^{-i2t} \sin^4(t/2)B_{p_0}$ is similar to the imperfect measurement operator discussed in Eq. (3) $\exp(\beta s_{p_0} B_{p_0}/2) = \cosh(\beta/2) + s_{p_0} \sinh(\beta/2)B_{p_0}$. However, there is an additional factor, which can be viewed as coherent errors appearing on data qubits. So while discussing error correction, aside from the consequence talked about before, coherent errors will do more damage to the error correction procedure and lead to worse performance. We also notice that under this realistic measurement model, if we define logical states by applying logical operators to the imperfect initial state, those states will not be orthogonal to each other, which makes it much hard to analyze theoretically.

In all, by mapping the standard QEC procedure under imperfect measurement to an SM model, we find two finite temperature phases that have different QEC performances. The high temperature (high physical error rate) phase signifies the failure of QEC caused by non-contractible error strings. In the

low temperature (low physical error rate) phase, the measurement errors cannot be identified through decoding syndrome outcomes of finite rounds due to imperfect initial state preparation, which could result in the failure of QEC in the large code distance limit. For finite d there will be a parameter region $\sim \log d$ that logical errors remain suppressed. In addition, we remark that studying a different measure of logical error rate, such as average gate fidelity [52] or diamond norm [24], might provide a better knowledge of how the results in this article affect error threshold in the current problem, which is very different since imperfect measurement of stabilizers not only causes faulty syndrome outcomes but also changes the quantum state as we discussed. Therefore, further work concerning these issues still needs to be developed. In addition, we notice that as shown in Ref. [43, 47], the imperfect initial state preparation leads to the absence of long-range entanglement. Meanwhile, the imperfect initial state is also the source of the ill performance in our QEC model. These phenomena are both related to the confinement of certain Wilson loop observables. Therefore, another intriguing question is that what role the long-range entanglement could play in the

threshold theorem of the general topological QEC codes?

ACKNOWLEDGMENTS

Authors thank Guo-Yi Zhu for the discussions on the finite-size effect of the SM model. We thank Jing-Yuan Chen, Li

Rao, and Qinghong Yang for helpful discussions. This work is partially supported by the Innovation Program for Quantum Science and Technology (Grant No. 2021ZD0302400) and Beijing Natural Science Foundation (Grant No. Z220002).

-
- [1] F. Arute, K. Arya, R. Babbush, and et al., *Nature* **574** (2019), [10.1038/s41586-019-1666-5](#).
 - [2] H.-S. Zhong, H. Wang, Y.-H. Deng, and et al., *Science* **370**, 1460 (2020).
 - [3] Y. Wu, W.-S. Bao, S. Cao, and et al., *Phys. Rev. Lett.* **127**, 180501 (2021).
 - [4] F. Arute, K. Arya, R. Babbush, and et al., *Science* **369**, 1084 (2020).
 - [5] M. Gong, S. Wang, C. Zha, and et al., *Science* **372**, 948 (2021).
 - [6] J. M. Pino, J. M. Dreiling, C. Figgatt, and et al., *Nature* **592**, 209 (2021).
 - [7] C. Ryan-Anderson and et al., (2021), [arXiv:2107.07505 \[quant-ph\]](#).
 - [8] J. Preskill, *Quantum* **2**, 79 (2018).
 - [9] P. W. Shor, *Phys. Rev. A* **52**, R2493 (1995).
 - [10] A. Steane, *Proc. R. Soc. Lond. A* **452**, 2551 (1996).
 - [11] A. R. Calderbank and P. W. Shor, *Phys. Rev. A* **54**, 1098 (1996).
 - [12] D. Nigg, M. Müller, E. A. Martinez, P. Schindler, M. Hennrich, T. Monz, M. A. Martin-Delgado, and R. Blatt, *Science* **345**, 302 (2014).
 - [13] N. Ofek, A. Petrenko, R. Heeres, P. Reinhold, Z. Leghtas, B. Vlastakis, Y. Liu, L. Frunzio, S. M. Girvin, L. Jiang, M. Mirrahimi, M. H. Devoret, and R. J. Schoelkopf, *Nature* **536**, 441 (2016).
 - [14] L. Hu, Y. Ma, W. Cai, X. Mu, Y. Xu, W. Wang, Y. Wu, H. Wang, Y. P. Song, C. L. Zou, S. M. Girvin, L.-M. Duan, and L. Sun, *Nature Physics* **15**, 503 (2019).
 - [15] C. K. Andersen, A. Remm, S. Lazar, S. Krinner, N. Lacroix, G. J. Norris, M. Gabureac, C. Eichler, and A. Wallraff, *Nature Physics* **16**, 875 (2020).
 - [16] A. Erhard, H. Poulsen Nautrup, M. Meth, L. Postler, R. Stricker, M. Stadler, V. Negnevitsky, M. Ringbauer, P. Schindler, H. J. Briegel, R. Blatt, N. Friis, and T. Monz, *Nature* **589**, 220 (2021).
 - [17] G. Q. Ai, *Nature* **595**, 383 (2021).
 - [18] Y.-H. Luo, M.-C. Chen, M. Erhard, H.-S. Zhong, D. Wu, H.-Y. Tang, Q. Zhao, X.-L. Wang, K. Fujii, L. Li, N.-L. Liu, K. Nemoto, W. J. Munro, C.-Y. Lu, A. Zeilinger, and J.-W. Pan, *Proceedings of the National Academy of Sciences* **118**, e2026250118 (2021).
 - [19] J. F. Marques, B. M. Varbanov, M. S. Moreira, H. Ali, N. Muthusubramanian, C. Zachariadis, F. Battistel, M. Beekman, N. Haider, W. Vlothuizen, A. Bruno, B. M. Terhal, and L. DiCarlo, *Nature Physics* **18**, 80 (2022).
 - [20] Y. Zhao and et al., *Phys. Rev. Lett.* **129**, 030501 (2022).
 - [21] C. Ryan-Anderson, J. G. Bohnet, K. Lee, D. Gresh, A. Hankin, J. P. Gaebler, D. Francois, A. Chernoguzov, D. Lucchetti, N. C. Brown, T. M. Gatterman, S. K. Halit, K. Gilmore, J. A. Gerber, B. Neyenhuis, D. Hayes, and R. P. Stutz, *Phys. Rev. X* **11**, 041058 (2021).
 - [22] L. Egan, D. M. Debroy, C. Noel, A. Risinger, D. Zhu, D. Biswas, M. Newman, M. Li, K. R. Brown, M. Cetina, and C. Monroe, *arXiv e-prints*, [arXiv:2009.11482 \(2020\)](#), [arXiv:2009.11482 \[quant-ph\]](#).
 - [23] E. Knill, R. Laflamme, and W. Zurek, *Proc. R. Soc. Lond. A* **454** (1998).
 - [24] D. Aharonov and M. Ben-Or, (1999), [arXiv:9906129 \[quant-ph\]](#).
 - [25] P. Aliferis, D. Gottesman, and J. Preskill, *Quant. Inf. Comput.* **6**, 97 (2006).
 - [26] M. A. Nielsen and I. L. Chuang, *Quantum computation and quantum information*, 1st ed. (Cambridge University Press, 2004).
 - [27] E. Dennis, A. Kitaev, A. Landahl, and J. Preskill, *Journal of Mathematical Physics* **43**, 4452 (2002).
 - [28] A. G. Fowler, M. Mariantoni, J. M. Martinis, and A. N. Cleland, *Phys. Rev. A* **86**, 032324 (2012).
 - [29] H. Bombin, (2013), [arXiv:1311.0277 \[quant-ph\]](#).
 - [30] D. Aharonov, A. Kitaev, and J. Preskill, *Phys. Rev. Lett.* **96**, 050504 (2006).
 - [31] C. T. Chubb and S. T. Flammia, *Ann. Inst. Henri Poincaré Comb. Phys. Interact.* **8** (2021), [10.4171/AIHPD/105](#).
 - [32] E. Novais, E. R. Mucciolo, and H. U. Baranger, *Phys. Rev. Lett.* **98**, 040501 (2007).
 - [33] E. Novais, E. R. Mucciolo, and H. U. Baranger, *Phys. Rev. A* **78**, 012314 (2008).
 - [34] J. P. Barnes, C. J. Trout, D. Lucarelli, and B. D. Clader, *Phys. Rev. A* **95**, 062338 (2017).
 - [35] S. J. Beale, J. J. Wallman, M. Gutiérrez, K. R. Brown, and R. Laflamme, *Phys. Rev. Lett.* **121**, 190501 (2018).
 - [36] S. Bravyi, M. Englbrecht, R. König, and N. Peard, *npj Quantum Information* **4** (2018), [10.1038/s41534-018-0106-y](#).
 - [37] E. Huang, A. C. Doherty, and S. Flammia, *Phys. Rev. A* **99**, 022313 (2019).
 - [38] Z. Cai, X. Xu, and S. C. Benjamin, *npj Quantum Information* **6** (2020), [10.1038/s41534-019-0233-0](#).
 - [39] Y. Ouyang, *npj Quantum Information* **7** (2021), [10.1038/s41534-021-00429-8](#).
 - [40] Y. Zhao and D. E. Liu, *arXiv e-prints*, [arXiv:2112.00473 \(2021\)](#), [arXiv:2112.00473 \[quant-ph\]](#).
 - [41] F. Venn, J. Behrends, and B. Béri, (2022), [arXiv:2211.00655 \[quant-ph\]](#).
 - [42] Q. Yang and D. E. Liu, *Physical Review A* **105**, 022434 (2022).
 - [43] G.-Y. Zhu, N. Tantivasadakarn, A. Vishwanath, S. Trebst, and R. Verresen, (2022), [arXiv:2208.11136 \[quant-ph\]](#).
 - [44] A. Kitaev, *Annals of Physics* **303**, 2 (2003).
 - [45] R. Acharya, I. Aleiner, R. Allen, and et al., (2022), [arXiv:2207.06431 \[quant-ph\]](#).
 - [46] See Supplemental Information for details of the derivation.
 - [47] J. Y. Lee, W. Ji, Z. Bi, and M. P. A. Fisher, (2022), [arXiv:2208.11699 \[cond-mat.str-el\]](#).
 - [48] J. B. Kogut, *Rev. Mod. Phys.* **51**, 659 (1979).
 - [49] H. Nishimori, *Progress of Theoretical Physics* **66**, 1169 (1981).
 - [50] H. Nishimori, *Statistical physics of spin glasses and informa-*

- tion processing: an introduction*, International series of monographs on physics No. 111 (Oxford University Press, 2001).
- [51] C. Wang, J. Harrington, and J. Preskill, *Annals of Physics* **303**, 31 (2003).
 - [52] J. Emerson, R. Alicki, and K. Å»yczkowski, *Journal of Optics B: Quantum and Semiclassical Optics* **7**, S347 (2005).
 - [53] C. Bény and O. Oreshkov, *Phys. Rev. Lett.* **104**, 120501 (2010).
 - [54] N. Tantivasadakarn, R. Thorngren, A. Vishwanath, and R. Verresen, (2021), [arXiv:2110.07599](https://arxiv.org/abs/2110.07599) [cond-mat.str-el].
 - [55] T. Ohno, G. Arakawa, I. Ichinose, and T. Matsui, *Nuclear Physics B* **697**, 462 (2004).
 - [56] A. Kitaev and J. Preskill, *Phys. Rev. Lett.* **96**, 110404 (2006).
 - [57] M. P. Harrigan and et al., *Nature Physics* **17**, 332 (2021).
 - [58] F. J. Wegner, *Journal of Mathematical Physics* **12**, 2259 (1971).
 - [59] S. Elitzur, *Phys. Rev. D* **12**, 3978 (1975).

Supplemental Information for "Lattice Gauge Theory and Topological Quantum Error Correction with Quantum Diversions in the Error Detection"

In this supplemental information, we provide details about derivations of the results in the main text. In Sec. SI we discuss some properties about code space when initial state preparation suffers from imperfection measurement. In Sec. SII we derive the SM mapping explicitly. In Sec. SIII we talk about the consequence of local symmetry under the Nishmori condition. In sec. SIV we derive the low-temperature expansion of the Wilson loop.

SI. CODE SUBSPACE UNDER IMPERFECT MEASUREMENT

Here we discuss the imperfect code subspace under the presence of coherent errors on entanglement gates during state preparation. Starting with a product state $\bigotimes_{e_0} |+\rangle_{e_0}$, we obtain the (unnormalized) state $M_{\{s_{p_0}\}} \bigotimes_{e_0} |+\rangle_{e_0}$ with probability

$$P(\{s_{p_0}\}) = \bigotimes_{e_0} \langle + |_{e_0} E_{\{s_{p_0}\}} \bigotimes_{e_0} | + \rangle_{e_0} = \frac{1}{(8 \cosh \beta)^N} \mathcal{Z}_{\{s_{p_0}\}}, \quad (\text{S1})$$

$$\mathcal{Z}_{\{s_{p_0}\}} = \sum_{\{\sigma_{e_0}\}} \exp \left[\beta \sum_{p_0} s_{p_0} b_{p_0} \right], b_{p_0} = \prod_{e_0 \in \partial p_0} \sigma_{e_0}, \quad (\text{S2})$$

where $M_{\{s_{p_0}\}}$ is the imperfect measurement operator

$$M_{\{s_{p_0}\}} = \frac{1}{(\sqrt{2} \cosh \beta)^N} \exp \left[\frac{1}{2} \beta \sum_{p_0} s_{p_0} B_{p_0} \right], \quad (\text{S3})$$

and $E_{\{s_{p_0}\}} = M_{\{s_{p_0}\}}^\dagger M_{\{s_{p_0}\}}$ is the corresponding POVM operator. By expanding $\bigotimes_{e_0} |+\rangle_{e_0}$ under computational basis $\bigotimes_{e_0} |+\rangle_{e_0} = (1/2^N) \sum_{\{\sigma_{e_0}\}} \bigotimes_{e_0} |\sigma_{e_0}\rangle$, where $\sigma_{e_0} = \pm 1$ is the eigenvalue of Pauli operator Z_{e_0} , it can be shown that $P(\{s_{p_0}\})$ is proportional to the partition function of a 2-d \mathbb{Z}_2 lattice gauge theory $\mathcal{Z}_{\{s_{p_0}\}}$ [1, 2], which is a useful method to dealing with the post-measurement state and is helpful to our following derivations. Note that 2-d \mathbb{Z}_2 lattice gauge theory is exact-solvable [3]. By noticing that the Boltzmann weight only depends on the value of b_{p_0} , we rewrite the summation of spin configurations as a summation of b_{p_0} configurations together with 1-form symmetry operations

$$\sum_{\{\sigma_{e_0}\}} = \sum_{\{b_{p_0}\}} \delta_{\prod_{p_0} b_{p_0}, 1} \sum_{\text{dual loop}}. \quad (\text{S4})$$

Here $\delta_{\prod_{p_0} b_{p_0}, 1}$ means that the product of all b_{p_0} must equal to 1, since the lattice is embedded in a torus surface. We may check the degree of freedoms involved in the summation $2^{2N} = 2^N / 2 \times 2^{N+1}$. Thus we have

$$\begin{aligned} \mathcal{Z}_{\{s_{p_0}\}} &= \sum_{\{b_{p_0}\}} \delta_{\prod_{p_0} b_{p_0}, 1} \sum_{\text{dual loop}} \exp \left[\beta \sum_{p_0} s_{p_0} b_{p_0} \right] \\ &= 2^{N+1} \sum_{\{b_{p_0}\}} \frac{1 + \prod_{p_0} b_{p_0}}{2} \exp \left[\beta \sum_{p_0} s_{p_0} b_{p_0} \right] \\ &= 2^N \prod_p \left(\sum_{b_{p_0}} \exp [\beta s_{p_0} b_{p_0}] + \sum_{b_{p_0}} b_{p_0} \exp [\beta s_{p_0} b_{p_0}] \right) \\ &= 2^N (2 \cosh \beta)^N + 2^N (2 \sinh \beta)^N \prod_{p_0} s_{p_0}, \end{aligned} \quad (\text{S5})$$

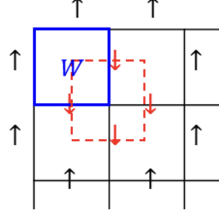


FIG. S1. 2-d \mathbb{Z}_2 lattice gauge theory. The classical spins σ_{e_0} are associated with each edge. Both the Hamiltonian and Wilson loop (blue solid loop) are invariant under 1-form symmetry operation (red dashed loop) which flips the spins on a dual loop.

and hence we have the probability of measurement outcomes

$$P(\{s_{p_0}\}) = \frac{1 + (\tanh \beta)^N \prod_p s_{p_0}}{2^N}. \quad (\text{S6})$$

Note that $\prod_{p_0} s_{p_0}$ is the parity of $\{s_{p_0}\}$ configuration.

From the above discussion, it can be seen that we might get different states with respect to the ancilla measurement outcome $\{s_{p_0}\}$. But we will fix the initial state as $M_{\{+\}} \otimes_{e_0} |+\rangle_{e_0}$, where we assumed the measurement outcomes of ancilla qubits are all +1. For other measurement outcomes $\{s_{p_0}\}$, we can redefine the sign of our stabilizers $B_{p_0} \rightarrow s_{p_0} B_{p_0}$ in order that the following discussions still apply. The only thing we should take into consideration is the parity of outcome $\{s_{p_0}\}$ because under the redefinition $\prod_{p_0} B_{p_0} = 1 \rightarrow \prod_{p_0} B_{p_0} = \prod_s s_{p_0}$ and we will get -1 for odd parity. In the odd parity case, the defects on the lattice cannot be paired up and it is unfriendly to error correction. Hence we ignore odd parity outcomes. We might consider it as a post-selection procedure, which chooses the even parity result that occurs with probability $P_+ = (1 + (\tanh \beta)^N)/2$, see Eq. (S6). We find that $1/2 \leq P_+ \leq 1$ for $0 \leq \beta \leq +\infty$. Note that this probability is close to 1 we β is sufficiently large, so the post-selection procedure is reasonable for experimental consideration.

Till now we have only obtained one logical state. What about other states in the imperfect code subspace? The problem is that the matrix rank of $M_{\{s_{p_0}\}}$ is 2^{2N} , which means that if we view it as a map defined on the whole 2^{2N} dimensional Hilbert space of physical qubits, $M_{\{s_{p_0}\}} : \mathcal{H} \rightarrow \mathcal{H}$, then we find that $\text{Im}(M_{\{s_{p_0}\}}) = \mathcal{H}$. This is different from the projective measurement case that $P_{\{s_{p_0}\}} = \prod_{p_0} (I + s_{p_0} B_{p_0})/2$ projects any states into the $B_{p_0} = s_{p_0}$ subspace. That is why we define the code space using logical operators in analogy to experimental setups. In summary, our four logical basis states are defined as

$$\begin{aligned} |\widetilde{++}\rangle &= \frac{M_{\{+\}} \otimes_{e_0} |+\rangle_{e_0}}{\sqrt{\otimes_{e_0} \langle +|_{e_0} M_{\{+\}}^\dagger M_{\{+\}} \otimes_{e_0} |+\rangle_{e_0}}}, \\ |\widetilde{-+}\rangle &= Z_{l_1} |\widetilde{++}\rangle, \quad |\widetilde{+-}\rangle = Z_{l_2} |\widetilde{++}\rangle, \quad |\widetilde{--}\rangle = Z_{l_1} Z_{l_2} |\widetilde{++}\rangle, \end{aligned} \quad (\text{S7})$$

Notice that $|\widetilde{++}\rangle$ state correspond to the model

$$\mathcal{Z}_{\{+\}} = \sum_{\{\sigma_{e_0}\}} \exp \left[\beta \sum_{p_0} b_{p_0} \right]. \quad (\text{S8})$$

Given the above imperfect logical states, the expectation value of Pauli Z operators can be computed through the classical SM model [1, 2]. We denote $\langle \cdot \rangle_{\{+\}}^q$ as the expectation value of the post-measurement state $|\widetilde{++}\rangle$, then

$$\left\langle \prod_{e_0 \in c_0} Z_{e_0} \right\rangle_{\{+\}}^q = \left\langle \prod_{e_0 \in c_0} \sigma_{e_0} \right\rangle_{\{+\}}^c. \quad (\text{S9})$$

where we denote c_0 as a set of several edges and $\langle \cdot \rangle_{\{+\}}^c$ as the expectation value of the classical model $\mathcal{Z}_{\{+\}}$.

2-d \mathbb{Z}_2 lattice gauge theory possesses 1-form symmetry [3]. As in Fig. S1, if we flip all the spins along a dual loop, it does not change the value of b_{p_0} on any plaquette p_0 , hence does not change the partition function, i.e. Eq. (S2).

For 2-d \mathbb{Z}_2 lattice gauge theory, Elitzur's theorem [3, 4] states that the expectation value of any observable that

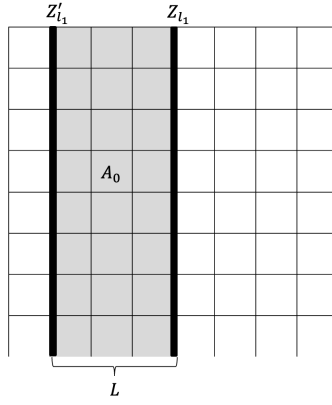


FIG. S2. Different definitions of logical Pauli Z operator. Under imperfect measurement preparation, the two logical states defined by them are different. The fidelity between these two states relates to the expectation value of a Wilson loop observable constituted by these two non-contractible loops.

varies under 1-form symmetry operation vanishes (even under the presence of infinitesimal source term). For example, consider the overlap between two logical states

$$\langle \widetilde{-+} | \widetilde{++} \rangle = \langle \widetilde{++} | Z_{l_1} | \widetilde{++} \rangle = \langle Z_{l_1} \rangle_{\{+\}}^q = \left\langle \prod_{e_0 \in l_1} \sigma_{e_0} \right\rangle_{\{+\}}^c. \quad (\text{S10})$$

The operator $\prod_{e_0 \in l_1} \sigma_{e_0}$ is the product σ_{e_0} spins that win around the non-contractible loop l_1 , and it changes sign under the 1-form symmetry operation that flips the spins on a dual non-contractible loop l_1^* that intersect with l_1 . Consequently, we find that $\langle \widetilde{-+} | \widetilde{++} \rangle = 0$. Note that this result can also be checked through explicit calculation since $\mathcal{Z}_{\{+\}}$ acquires an exact solution. Similarly, we find that all the four states $\{|\widetilde{++}\rangle, |\widetilde{-+}\rangle, |\widetilde{+-}\rangle, |\widetilde{--}\rangle\}$ are orthogonal to each other. Therefore, they form an orthonormal basis of a 4 dimensional subspace. This justifies our definition of the imperfect code subspace

$$\tilde{\mathcal{C}}(\beta) = \text{span}\{|\widetilde{++}\rangle, |\widetilde{-+}\rangle, |\widetilde{+-}\rangle, |\widetilde{--}\rangle\} \quad (\text{S11})$$

What is more, these four states are still eigenstates of logical X operators. Since $X_{l_1^*}, X_{l_2^*}$ commute with imperfect measurement operator $M_{\{+\}}$ and act as 1 on the initial product state, we find that $X_{l_1^*} |\widetilde{++}\rangle = |\widetilde{++}\rangle, X_{l_2^*} |\widetilde{++}\rangle = |\widetilde{++}\rangle$. The act on the other three states is determined by the commutation relation between logical X and logical Z . Note that these properties are not universal for imperfect measurement but depend on the specific measurement protocol.

Here we point out that, unlike the projective measurement case, $\tilde{\mathcal{C}}$ depends on the choice of logical operators on the lattice. For example, consider a different choice of logical Z operator Z'_{l_1} as in Fig. S2. We can calculate the fidelity between $|\widetilde{-+}\rangle$ and the new state defined by the new logical operator $|\widetilde{-+}\rangle' = Z'_{l_1} |\widetilde{++}\rangle$:

$$\langle \widetilde{-+} | \widetilde{-+} \rangle' = \langle \widetilde{++} | Z_{l_1} Z'_{l_1} | \widetilde{++} \rangle = \langle Z_{l_1} Z'_{l_1} \rangle_{\{+\}}^q \quad (\text{S12})$$

Note that $Z_{l_1} Z'_{l_1}$ forms a Wilson loop that could be written as the boundary of a region A . For the classical model, Wilson loops are 1-form symmetry invariant observables and acquire non-zero expectation values. For example, consider the Wilson loop

$$W_{A_0} = \prod_{p_0 \in A_0} b_{p_0} = \prod_{e_0 \in \partial A_0} \sigma_{e_0}, \quad (\text{S13})$$

where A_0 is a 2-d region (a set of plaquettes) and ∂A_0 is the set of edges at the boundary of A_0 . Its expectation value can be evaluated similarly as the partition function, which leads to

$$\langle W_{A_0} \rangle_{\{+\}}^c = \frac{(\tanh \beta)^{|A_0|} + (\tanh \beta)^{N-|A_0|}}{1 + (\tanh \beta)^N}. \quad (\text{S14})$$

With the help of Eq. (S14), we obtain:

$$\langle \widetilde{-+} | \widetilde{-+} \rangle' = \frac{(\tanh \beta)^{dL} + (\tanh \beta)^{N-dL}}{1 + (\tanh \beta)^N} \quad (\text{S15})$$

which is smaller than 1 for finite β , implies that the two states are different.

In addition, notice that we can take the product of the eigenstates of $N-1$ B_{p_0} operators, $N-1$ A_{v_0} operators, and 2 logical operators $X_{l_1^*}$ and $X_{l_2^*}$ to form a complete basis of the whole Hilbert space of physical qubits. Under this basis the product $|+\rangle$ state can be written as

$$\bigotimes_{e_0} |+\rangle_{e_0} = \bigotimes_{p_0}' \sum_{b_{p_0}=\pm} |B_{p_0}=b_{p_0}\rangle \bigotimes_{v_0}' |A_{v_0}=+\rangle \bigotimes |X_{l_1^*}=+\rangle \bigotimes |X_{l_2^*}=+\rangle, \quad (\text{S16})$$

Here the prime on the product symbol means that a chosen plaquette or vertex is excluded to satisfy the global constrain $\prod_{p_0} B_{p_0} = \prod_{v_0} A_{v_0} = I$. This formula is verified as follows. Since the action of A_{v_0} 's and logical X operators on $\bigotimes_{e_0} |+\rangle_{e_0}$ all yield +1, the state must be the +1 eigenstate of these operators. Besides, assume the excluded plaquette is f_0 . Consider a Pauli X string $X_{(f_0 \rightarrow q_0)}$ that starts at f_0 and ends at some other plaquette q_0 . Since $X_{(f_0 \rightarrow q_0)}$ commutes with all $N-1$ A_{v_0} operators, logical X operators and $N-2$ B_{p_0} 's with $p_0 \neq q_0, f_0$, it only acts on the factor $|B_{q_0}=\pm\rangle$ under the above basis. Note that $X_{(f_0 \rightarrow q_0)}$ anti-commutes with B_{q_0} , so $X_{(f_0 \rightarrow q_0)} |B_{q_0}=\pm\rangle = |B_{q_0}=\mp\rangle$. Since $X_{(f_0 \rightarrow q_0)} \bigotimes_{e_0} |+\rangle_{e_0} = \bigotimes_{e_0} |+\rangle_{e_0}$, the product state must be stabilized by $X_{(f_0 \rightarrow q_0)}$. Applying such X strings to all the plaquettes, we find that $\bigotimes_{e_0} |+\rangle_{e_0}$ is the +1 eigenstate of $X_{(f_0 \rightarrow q_0)}$ for all $q_0 \neq f_0$, which leads to Eq. (S16). With the above considerations, we find that the imperfect measurement operator $M_{\{s_{p_0}\}}$ only acts on the stabilizer bits ($|B_{p_0}=\pm\rangle$ and $|A_{v_0}=\pm\rangle$) and logical operators only act on the logical bits ($|X_{l_1^*}=\pm\rangle$ and $|X_{l_2^*}=\pm\rangle$). Consequently, any state $|\tilde{\Psi}\rangle$ in the code space $\tilde{\mathcal{C}}$ can be expanded under the stabilizer basis to achieve the form:

$$|\tilde{\Psi}\rangle \propto \left[\exp\left(\frac{\beta}{2} \prod_{p_0}' B_{p_0}\right) \bigotimes_{p_0}' \sum_{b_{p_0}=\pm} \exp\left(\frac{\beta}{2} b_{p_0}\right) |B_{p_0}=b_{p_0}\rangle \right] \left[\bigotimes_{v_0}' |A_{v_0}=+\rangle \right] \bigotimes |L\rangle, \quad (\text{S17})$$

where $|L\rangle$ represents the logical qubits and is exactly where the logical information is stored.

SIII. DERIVATION OF STATISTICAL MECHANICAL MAPPING

Recall that we have considered a multi-round error correction protocol [5] under imperfect syndrome measurement, listed as follows:

1. start with an arbitrary state $|\tilde{\Psi}\rangle$ in $\tilde{\mathcal{C}}(\beta_0)$.
2. Probabilistic Pauli X error acts at each integer valued time $t = 1, 2, \dots, T$. The X error at each physical qubit on each time slice occurs independently with probability q . Denote the error chain at time t as $c_0^*(t)$. $c_0^*(t)$ is a set of edges, where the star reminds us that it will be viewed as strings on the dual lattice. The associated Pauli operator is $X_{c_0^*(t)} = \prod_{e_0 \in c_0^*(t)} X_{e_0}$.
3. Perform a round of syndrome measurement between each time interval $[t, t+1]$. The syndrome measurements are also imperfect and their strength of measurement is set as β . Suppose the measurement outcome at time interval $[t, t+1]$ is $\{s_{p_0}(t)\}$, then the associated action of imperfect measurement is $M_{\{s_{p_0}(t)\}}$.
4. After T rounds of syndrome measurements, we decode and apply Pauli X correction to the final state. Denote the correction chain as c_{0R}^* and corresponding correction operator as $X_{c_{0R}^*}$.

Notice that with our definition of code space $\tilde{\mathcal{C}}$, the imperfection of syndrome measurement only affects syndrome bits but does not disturb logical information. We have known that any state in $\tilde{\mathcal{C}}$ takes the form as shown in Eq. (S17). Acting successive imperfect measurement operators on it still only affects the stabilizer bits. The logical information $|L\rangle$ will be left unchanged.

We might represent our error correction procedure as a diagram in Fig. 3(a). We will show that when the error chains at all times and the correction chain together constitute a contractible loop (correction operator and Pauli error

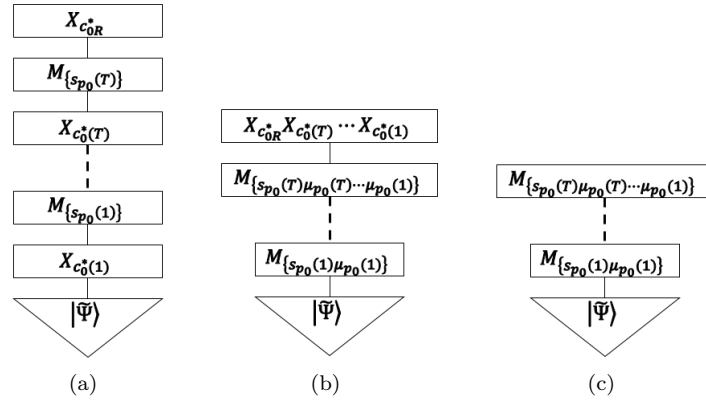


FIG. S3. Diagrams for error correction procedure. The bottom triangle is the initial state. The squares above represent actions of Pauli errors and imperfect measurements. (a) Original error correction procedure. Pauli errors and imperfect measurements act repetitiously. (b) Move Pauli error operators to the top making use of the commutation relation, i.e. Eq. (S18). (c) When the correction operator and Pauli error operators form a stabilizer, they together commute with imperfect measurement operators and hence have no effect on the final state.

operators forms stabilize) the logical information is still preserved. Notice that the commutation between $M_{\{s_{p_0}(t)\}}$ and Pauli error $X_{c_0^*}^*(t')$ can be expressed as

$$M_{\{s_{p_0}(t)\}} X_{c_0^*}^*(t') = X_{c_0^*}^*(t') M_{\{s_{p_0}(t)\mu_{p_0}(t')\}}. \quad (\text{S18})$$

Here $\{\mu_{p_0}(t')\}$ represents the correct syndrome that should be generated by Pauli error $X_{c_0^*}^*(t')$. In other words $\mu_{p_0}(t') = -1$ when p locates at the boundary of c_0^* and $\mu_{p_0}(t') = 1$ otherwise. Using this commutation relation we can move all Pauli error chains in Fig. 3(a) to the top and arrive at Fig. 3(b). When the operator $X_{c_0^*}^* X_{c_0^*}^*(T) \cdots X_{c_0^*}^*(1)$ forms a product of A_{v_0} operators, it will be commuting with imperfect measurement operators and logical Pauli operators, and hence acts trivially on the state below. Therefore we will obtain a final state as in Fig. 3(c). Though the final state is different from the original state $|\tilde{\Psi}\rangle$, it will be containing the same logical information, so we view this situation as a success of error correction.

Then we may compute the probability of syndrome outcomes given a particular error configuration $\{c_0^*(t)\}$

$$\begin{aligned} P(\{s_{p_0}(t)\}|\{c_0^*(t)\}) &= \|\prod_t M_{\{s_{p_0}(t)\}} X_{c_0^*}^*(t) |\tilde{\Psi}\rangle\|^2 \\ &= \|\prod_t M_{\{s_{p_0}(t)\} \prod_{k \leq t} \mu_{p_0}(k)} |\tilde{\Psi}\rangle\|^2 = \langle \tilde{\Psi} | \prod_t E_{\{s_{p_0}(t)\} \prod_{k \leq t} \mu_{p_0}(k)} |\tilde{\Psi}\rangle. \end{aligned} \quad (\text{S19})$$

Here $\|\cdot\|^2$ denotes the state norm. First, note that this expression is a well-defined joint probability for the $s_{p_0}(t)$ variables. $P(\{s_{p_0}(t)\}|\{c_0^*(t)\})$ is always non-negative, and it is normalized as $\sum_{\{s_{p_0}(t)\}} P(\{s_{p_0}(t)\}|\{c_0^*(t)\}) = 1$, which could be verified by applying the normalization of POVM operators $\sum_{\{s_{p_0}\}} E_{\{s_{p_0}\}} = I$ for each time slice. Besides, we can check that it is the true probability of syndrome measurements on the physical level. For example, imagine we are performing error correction in real world. At the time t' , we ask what is the syndrome measurement probability for the current step. Eq. (S19) tells us that it should be a probability at the t' step conditioned on the configurations of previous steps

$$\begin{aligned} P(\{s_{p_0}(t=t')\}|\{s_{p_0}(t < t')\}, \{c_0^*(t)\}) &= \frac{\sum_{\{s_{p_0}(t > t')\}} P(\{s_{p_0}(t)\}|\{c_0^*(t)\})}{\sum_{\{s_{p_0}(t \geq t')\}} P(\{s_{p_0}(t)\}|\{c_0^*(t)\})} = \frac{\|\prod_{t \leq t'} M_{\{s_{p_0}(t)\}} X_{c_0^*}^*(t) |\tilde{\Psi}\rangle\|^2}{\|\prod_{t < t'} M_{\{s_{p_0}(t)\}} X_{c_0^*}^*(t) |\tilde{\Psi}\rangle\|^2} \\ &= \frac{\text{tr}(E_{\{s_{p_0}(t')\}} \rho)}{\text{tr}(\rho)}, \quad \rho = \left(X_{c_0^*}^*(t') \prod_{t < t'} M_{\{s_{p_0}(t)\}} X_{c_0^*}^*(t) \right) |\tilde{\Psi}\rangle \langle \tilde{\Psi}| \left(X_{c_0^*}^*(t') \prod_{t < t'} M_{\{s_{p_0}(t)\}} X_{c_0^*}^*(t) \right)^\dagger. \end{aligned} \quad (\text{S20})$$

We arrive at the actual POVM probability at the current error correction step. Note that it also does not depend on

the Pauli errors after time t' . Calculate the expression in Eq. (S19) explicitly, we have

$$\begin{aligned} P(\{s_{p_0}(t)\}|\{c_0^*(t)\}) &= \frac{1}{\mathcal{Z}_{\{+\}} \sum_{\{\sigma_{e_0}\}} e^{\beta_0 \sum_{p_0} b_{p_0}} \prod_{p_0, t} \frac{\exp(\beta b_{p_0} s_{p_0}(t) \prod_{k \leq t} \mu_{p_0}(k))}{2 \cosh \beta}} \\ &= \frac{1}{\mathcal{Z}_{\{+\}} (2 \cosh \beta)^{NT}} \sum_{\{\sigma_{e_0}\}} \exp \left[\sum_{p_0} b_{p_0} \left(\beta_0 + \beta \sum_t s_{p_0}(t) \prod_{k \leq t} \mu_{p_0}(k) \right) \right]. \end{aligned} \quad (\text{S21})$$

Here $\mathcal{Z}_{\{+\}} = 4^N (\cosh^N \beta_0 + \sinh^N \beta_0)$ is the partition function of 2-d \mathbb{Z}_2 lattice gauge theory. The σ_{e_0} 's have the same origin as Eq. (S2) through expansion under computational basis. Note that the above expression is independent of the choice of $|\tilde{\Psi}\rangle$ in code space. This can be shown by expanding $|\tilde{\Psi}\rangle$ under logical basis $|\tilde{\Psi}\rangle = \Psi_{++} |++\rangle + \Psi_{+-} |+-\rangle + \Psi_{-+} |-+\rangle + \Psi_{--} |--\rangle$ and using Elitzur's theorem. Since the POVM operators $E_{s_{p_0}(t)}$ at different times and different plaquettes are all complete and commute with each other, we may view the above probability as a joint probability of syndrome outcomes at different spacetime points, and it is conditioned on the error configuration. Notice that the syndromes at different times are correlated by the physical spin σ_{e_0} . That is because the imperfect measurement at each time step alters the instant quantum state, which affects the syndrome probability at the next time step. We can also construct a joint probability for both syndrome outcomes and error configuration. Noticing that the probability of a given error configuration is

$$P(\{c_0^*(t)\}) = \prod_{e_0, t} q^{\frac{1+\eta_{e_0}(t)}{2}} (1-q)^{\frac{1-\eta_{e_0}(t)}{2}} = \prod_{e_0, t} \frac{\exp(K \eta_{e_0}(t))}{2 \cosh K}, \quad (\text{S22})$$

we have

$$\begin{aligned} P(\{s_{p_0}(t)\}, \{c_0^*(t)\}) &= P(\{s_{p_0}(t)\}|\{c_0^*(t)\}) P(\{c_0^*(t)\}) \\ &= \frac{1}{\mathcal{Z}_{\{+\}} \prod_{e_0, t} \frac{\exp(K \eta_{e_0}(t))}{2 \cosh K}} \sum_{\{\sigma_{e_0}\}} e^{\beta_0 \sum_{p_0} b_{p_0}} \prod_{p, t} \frac{\exp(\beta b_{p_0} s_{p_0}(t) \prod_{k \leq t} \prod_{e_0 \in \partial p_0} \eta_{e_0}(k))}{2 \cosh \beta} \\ &= \frac{1}{\mathcal{Z}_{\{+\}} (2 \cosh \beta)^{NT} (2 \cosh K)^{2NT}} \sum_{\{\sigma_{e_0}\}} \exp \left[K \sum_{e_0, t} \eta_{e_0}(t) + \sum_{p_0} b_{p_0} \left(\beta_0 + \beta \sum_t s_{p_0}(t) \prod_{k \leq t} \prod_{e_0 \in \partial p_0} \eta_{e_0}(k) \right) \right] \\ &\equiv P(\{s_{p_0}(t)\}, \{\eta_{e_0}(t)\}). \end{aligned} \quad (\text{S23})$$

Here $K = -\frac{1}{2} \ln \frac{q}{1-q}$ and $\eta_{e_0}(t) = \pm 1$ signs the presence of Pauli error, which means $\eta_{e_0}(t) = -1$ if the error configuration $\{c_0^*(t)\}$ includes edge e_0 at time t and $\eta_{e_0}(t) = +1$ otherwise. Besides the boundary configuration of an error chain $c_0^*(t)$ can also be represented by $\eta_{e_0}(t)$, that is $\mu_{p_0}(t) = \prod_{e_0 \in \partial p_0} \eta_{e_0}(t)$.

Then we shall discuss in detail how could we decode with the syndrome outcomes $\{s_{p_0}(t)\}$. We mainly follow the method used in Ref. [5]. It is convenient to consider the situation that our logical information is stored forever. We extend the initial time $t = 1$ to $-\infty$ and the final time $t = T$ to $+\infty$, which means that the syndrome measurement procedure is performed forever without beginning or end. The error correction procedure is represented as a 3 dimensional lattice in Fig. S4. The vertical plaquettes represent physical qubits at different times and the horizontal plaquettes mark syndrome outcomes. The Pauli X errors are associated with vertical plaquettes (horizontal dashed lines), and the measurement errors are associated with horizontal plaquettes (vertical dashed lines). A given syndrome forms a chain in 3-d spacetime, and we denote the syndrome chain as c_S^* . Note that c_S^* is a set of spacetime plaquettes, and we view it as a chain on the dual lattice (dashed lines in Fig. S4). We can also view it as a \mathbb{Z}_2 valued vector with all the plaquettes as its basis. The task of the decoder is to find out both measurement errors and Pauli errors with respect to the information of syndrome c_S^* . Denote the error chain of both measurement and Pauli errors as c_E^* , it obvious that c_E^* should have the same boundary as c_S^* , $\partial^* c_S^* = \partial^* c_E^*$. Here $\partial^* c_S^*$ is the set of cubics where the boundary points of c_S^* lie in. Suppose the error chain decided by the decoder is $c_{E'}^*$, when $c_{E'}^*$ and c_E^* are homologically equivalent, which means $c_{E'}^* + c_E^*$ forms contractible loop (here the plus is defined mod \mathbb{Z}_2), it should make no difference when we finally apply correction operator at $t = +\infty$, hence the error correction will be successful. But if $c_{E'}^* + c_E^*$ forms contractible loops, then the corresponding correction operator will be containing logical X operator which has a nontrivial influence on logical information. In that case, the error correction will fail. So the task of the optimal decoder, named as maximum likelihood decoder, is to identify the equivalent class of error chains with the largest probability. Here the equivalent class of an error chain $[c_E^*]$ is defined as the set of all error chains

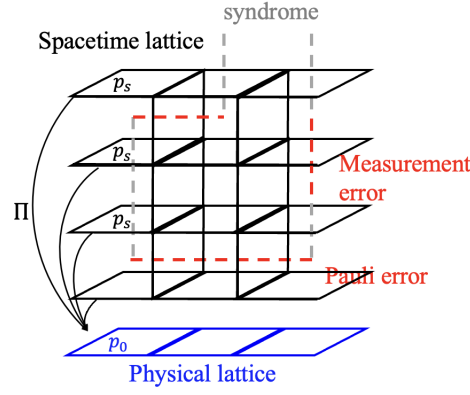


FIG. S4. 3-d spacetime of error history. The black lattice is the spacetime lattice, which takes periodic boundary condition at space directions and infinite boundary condition at time direction. The Pauli errors, measurement errors and error syndrome are represented as strings on the dual lattice (dashed lines). The horizontal red strings crossing timelike (vertical) plaquettes represent the locations of Pauli X errors which actually act on the physical lattice (blue). The vertical gray strings crossing spacelike (horizontal) plaquettes represent the error syndrome, which marks the locations of measurement results $s_{p_0}(t) = -1$ at different time steps. The vertical red strings are where error syndromes do not match the Pauli errors that actually occurred, which we view as measurement errors. Π denotes the projection from the 3-d spacetime lattice to the 2-d physical lattice.

that are homologically equivalent to c_E^* .

The probability of error chain class could be derived from Eq. (S23). Notice that measurement error configuration can be inferred from the syndrome at that moment and error configuration in the past

$$\eta_{p_0}(t) = s_{p_0}(t) \prod_{k \leq t} \mu_{p_0}(k) = s_{p_0}(t) \prod_{k \leq t} \prod_{e_0 \in \partial p_0} \eta_{e_0}(k). \quad (\text{S24})$$

Substitute the above equation into Eq. (S23), we obtain the joint probability of both measurement and Pauli error

$$P(\{\eta_{p_0}(t)\}, \{\eta_{e_0}(t)\}) = \frac{1}{\mathcal{Z}_{\{+\}} \prod_t [(2 \cosh \beta)^N (2 \cosh K)^{2N}]} \times \sum_{\{\sigma_{e_0}\}} \exp \left[K \sum_{e,t} \eta_{e_0}(t) + \sum_{p_0} b_{p_0} \left(\beta_0 + \beta \sum_t \eta_{p_0}(t) \right) \right]. \quad (\text{S25})$$

In this expression, we see that measurement errors at different time steps are correlated. Generally, the presence of measurement error increases the probability of measurement error at later times. We reinterpret the above equation on the 3-d lattice. Given an error chain in 3-d spacetime c_E^* , we still mark the location of error as $\eta_p = -1$. Specifically, measurement error at a spacelike plaquette is denoted as $\eta_{p_s} = -1$. Pauli error at a timelike plaquette is denoted as $\eta_{p_t} = -1$. Then the probability of the error chain is expressed as

$$P(c_E^*) = P(\{\eta_p\}) = \frac{1}{\mathcal{Z}_{\{+\}} \prod_t [(2 \cosh \beta)^N (2 \cosh K)^{2N}]} \times \sum_{\{\sigma_{e_0}\}} \exp \left[K \sum_{p_t} \eta_{p_t} + \beta_0 \sum_{p_0} b_{p_0} + \beta \sum_{p_s} b_{\Pi(p_s)} \eta_{p_s} \right]. \quad (\text{S26})$$

Note that σ_{e_0} 's and associated b_{p_0} 's are viewed as lying on a 2-d lattice distinct from the 3-d spacetime representing error correction history. Each p_s is associated with an $b_{\Pi(p_s)}$ on the 2-d physical lattice such that p_s and $\Pi(p_s)$ correspond to the same space point as in Fig. S4.

The probability of error class $[c_E]$ is calculated as a summation of probabilities of error chains that belong to the same equivalent class:

$$P([c_E]) = \sum_{c \in [c_E]} P(c) \quad (\text{S27})$$

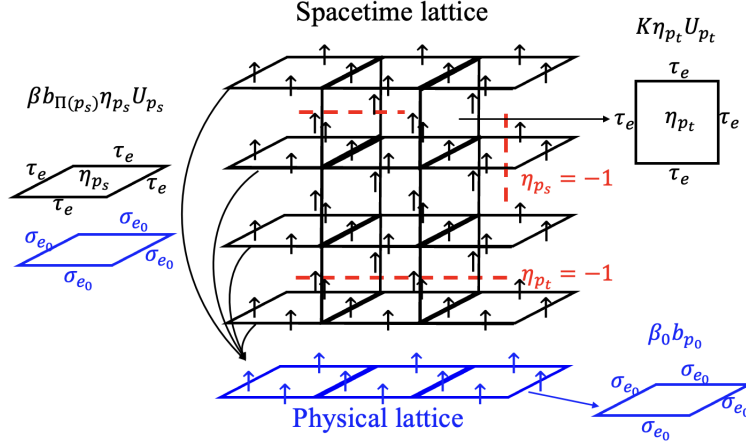


FIG. S5. Illustration of the SM model we obtained. The τ_e spins are defined on the edges of 3-d spacetime lattice and the σ_{e_0} . There are three types of interactions in this model. $\beta_0 b_{p_0}$ is the gauge interaction term defined on the physical lattice. $K \eta_{p_t} U_{p_t}$ is the timelike gauge interaction on spacetime lattice. The $\beta b_{\Pi(p_s)} \eta_{p_s} U_{p_s}$ term couples the spacelike gauge interaction term U_{p_s} to the gauge interaction term $b_{\Pi(p_s)}$ on physical lattice. The η_p 's set the signs of gauge interactions on the spacetime lattice.

This summation can be done by introducing virtual spin $\tau_p = \pm 1$ associated with each spacetime plaquette and relating it to each edge through \mathbb{Z}_2 gauge interaction [5], as in Fig. S5. The summation of homologically equivalent error chains yields the same result as the summation of configurations of virtual spins τ_e defined on edges up to a factor counting the number of 1-form symmetry operations since the sign changing of τ_e corresponds to a deformation of error chain (see Fig. S6) and thus relates homologically equivalent error chains.:

$$\begin{aligned}
 P([c_E]) &= \frac{1}{\mathcal{N}_1} \sum_{\{\tau_p\}} P(\{\eta_p \prod_{e \in \partial p} \tau_e\}) \\
 &= \frac{1}{\mathcal{N}_1 \mathcal{Z}_{\{+\}} \prod_t [(2 \cosh \beta)^N (2 \cosh K)^{2N}]} \\
 &\times \sum_{\{\sigma_{e_0}\}, \{\tau_e\}} \exp \left[\beta_0 \sum_{p_0} b_{p_0} + \beta \sum_{p_s} \left(b_{\Pi(p_s)} \eta_{p_s} \prod_{e \in \partial p_s} \tau_e \right) + K \sum_{p_t} \left(\eta_{p_t} \prod_{e \in \partial p_t} \tau_e \right) \right].
 \end{aligned} \tag{S28}$$

Here \mathcal{N}_1 denotes the number of 1-form symmetry operations and it diverges for infinite time T . We now arrive at an SM model including both virtual spins $\{\tau_p\}$ on the 3-d spacetime lattice and physical spins $\{\sigma_{e_0}\}$ on a distinct 2-d space lattice. The virtual spins in this SM model describe the fluctuation of error chains in the same class. The physical spins are coupled to virtual spins on time-like plaquettes at all times since the probability of measurement errors at a certain time depends on the entire syndrome measurement history. The optimal decoding algorithm should select the error class $[c_E]$ with the largest $P([c_E])$. Moreover, if the interaction configuration $\{\eta_e\}$ is viewed as disordered with a correlated probability distribution $P(\{\eta_e\})$ defined in equation S26, then the deconfinement-confinement phase transition point of virtual spins $\{\tau_p\}$ in this disordered SM model should signify the error threshold of the error correction protocol as discussed in Ref. [5]. In summary, the quenched disordered SM model describing the error threshold is

$$\begin{aligned}
 \mathcal{Z}(\{\eta_p\}) &= \sum_{\{\sigma_{e_0}\}, \{\tau_e\}} \exp \left[\beta_0 \sum_{p_0} b_{p_0} + \beta \sum_{p_s} b_{\Pi(p_s)} \eta_{p_s} U_{p_s} + K \sum_{p_t} \eta_{p_t} U_{p_t} \right], \\
 U_p &= \prod_{e \in \partial p} \tau_e, \quad b_{p_0} = \prod_{e_0 \in \partial p_0} \sigma_{e_0}, \\
 P(\{\eta_e\}) &= \frac{\sum_{\{\sigma_{e_0}\}} \exp \left[\beta_0 \sum_{p_0} b_{p_0} + \beta \sum_{p_s} b_{\Pi(p_s)} \eta_{p_s} + K \sum_{p_t} \eta_{p_t} \right]}{\mathcal{Z}_{\{+\}} \prod_t [(2 \cosh \beta)^N (2 \cosh K)^{2N}]}.
 \end{aligned} \tag{S29}$$

Note that in our SM model, all the spacelike plaquettes are coupled with the σ_{e_0} 's, causing a highly non-local corre-

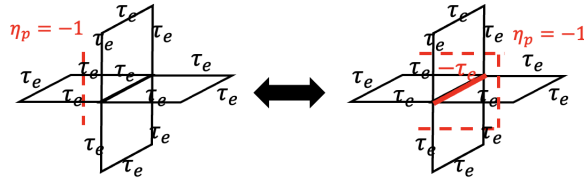


FIG. S6. Example of local symmetry. The red dashed lines represent the position where $\eta_p = -1$. The two $\{\eta_p\}$ configurations yield the same partition function by redefining the spin colored red. Pictorially, flipping τ_e spins is equivalent to a deformation of error chain.

lation in the timelike direction. This is a consequence of the imperfect measurement in the initial state preparation. When the initial state is well prepared $\beta_0 \rightarrow +\infty$, all the b_{p_0} 's will be set to +1 in Eq. (S29) and we arrive at a random plaquette gauge model:

$$\begin{aligned} \mathcal{Z}(\{\eta_p\}) &= \sum_{\{\sigma_{e_0}\}, \{\tau_e\}} \exp \left[\beta \sum_{p_s} \eta_{p_s} U_{p_s} + K \sum_{p_t} \eta_{p_t} U_{p_t} \right], \\ U_p &= \prod_{e \in \partial p} \tau_e, \\ P(\{\eta_e\}) &= \frac{\exp \left[K \sum_{p_t} \eta_{p_t} + \beta \sum_{p_s} \eta_{p_s} \right]}{\prod_t [(2 \cosh \beta)^N (2 \cosh K)^{2N}]}, \end{aligned} \quad (\text{S30})$$

which is derived in Ref. [5] to describe the error threshold under probabilistic measurement error.

From Eq. (S29) we can sum the σ_e 's out and arrive at the SM model containing pure τ_e spins

$$\begin{aligned} \mathcal{Z}(\{\eta_p\}) &= \sum_{\{\tau_e\}} \left[\prod_{p_0} \cosh(\beta_0 + \beta \sum_t \eta_{p_s} U_{p_s}) + \prod_{p_0} \sinh(\beta_0 + \beta \sum_t \eta_{p_s} U_{p_s}) \right] \exp \left[K \sum_{p_t} \eta_{p_t} \right], \\ P(\{\eta_e\}) &= \frac{1}{[(\cosh \beta_0)^N + (\sinh \beta_0)^N] \prod_t [(2 \cosh \beta)^N (2 \cosh K)^{2N}]} \\ &\times \left[\prod_{p_0} \cosh(\beta_0 + \beta \sum_t \eta_{p_s}) + \prod_{p_0} \sinh(\beta_0 + \beta \sum_t \eta_{p_s}) \right] \exp \left[K \sum_{p_t} \eta_{p_t} \right]. \end{aligned} \quad (\text{S31})$$

SIII. LOCAL SYMMETRY ON NISHIMORI LINE

The SM model $\mathcal{Z}(\{\eta_p\})$ has a local symmetry when redefining the interaction background $\{\eta_p\}$

$$\eta_p \rightarrow \eta_p \prod_{e \in \partial p} \nu_e, \quad \tau_e \rightarrow \tau_e \nu_e, \quad \nu_e = \pm 1. \quad (\text{S32})$$

as in Fig. S6. More precisely, the partition function is invariant under redefinition of background interaction configuration $\{\eta_p\}$:

$$\mathcal{Z}(\{\eta_p \prod_{e \in \partial p} \nu_e\}) = \mathcal{Z}(\{\eta_p\}) \quad (\text{S33})$$

since the influence is absorbed in the summation of spin configuration by redefining spin variable $\tau'_e = \tau_e \nu_e$. Note that $\{\eta_p\}$ correspond to a representative error chain in error class $[c_E]$, and the local invariance Eq. (S32) tells us that $\mathcal{Z}(\{\eta_p\})$ does not depend on the choice of representative error chain. It only depends on the homological class of error chain.

We will use the local invariance S32 on Nishimori line to derive several results about the phase structure [6, 7]. Under the presence of disorder, to compute an expectation value, we should first take the ensemble average for a particular interaction configuration (denoted by $\langle \cdot \rangle_{\{\eta_p\}}$) and then take the disorder average on different configurations (denoted

as $[\cdot]$). For a given observable $O(\{\eta_p\}, \{\sigma_{e_0}\}, \{\tau_e\})$ depending on the σ spins, τ spins and interaction configuration, these two kinds of averages are defined as:

$$\begin{aligned} \langle O \rangle_{\{\eta_p\}} &= \frac{1}{\mathcal{Z}(\{\eta_p\})} \sum_{\{\sigma_{e_0}\}, \{\tau_e\}} O \exp \left[\beta_0 \sum_{p_0} b_{p_0} + \beta \sum_{p_s} b_{\Pi(p_s)} \eta_{p_s} U_{p_s} + K \sum_{p_t} \eta_{p_t} U_{p_t} \right] \\ [\langle O \rangle_{\{\eta_p\}}] &= \sum_{\{\eta_p\}} P(\{\eta_p\}) \langle O \rangle_{\{\eta_p\}} \end{aligned} \quad (\text{S34})$$

If an observable $O(\{\eta_p\}, \{\sigma_{e_0}\}, \{\tau_e\})$ is also invariant under local symmetry transformation in Eq. (S32):

$$O(\{\eta_p \prod_{e \in \partial p} \nu_e\}, \{\sigma_{e_0}\}, \{\tau_e \nu_e\}) = O(\{\eta_p\}, \{\sigma_{e_0}\}, \{\tau_e\}) \quad (\text{S35})$$

then the expectation value can be evaluated as:

$$\begin{aligned} [\langle O \rangle] &= \sum_{\{\eta_p\}} \frac{P(\{\eta_p\})}{\mathcal{Z}(\{\eta_p\})} \sum_{\{\sigma_{e_0}\}, \{\tau_e\}} O(\{\eta_p\}, \{\sigma_{e_0}\}, \{\tau_e\}) \\ &\times \exp \left[\beta_0 \sum_{p_0} b_{p_0} + \beta \sum_{p_s} b_{\Pi(p_s)} \eta_{p_s} U_{p_s} + K \sum_{p_t} \eta_{p_t} U_{p_t} \right] \\ &= \sum_{\{\eta_p\}} \frac{P(\{\eta_p \prod_{e \in \partial p} \nu_e\})}{\mathcal{Z}(\{\eta_p \prod_{e \in \partial p} \nu_e\})} \sum_{\{\sigma_{e_0}\}, \{\tau_e\}} O(\{\eta_p \prod_{e \in \partial p} \nu_e\}, \{\sigma_{e_0}\}, \{\tau_e\}) \\ &\times \exp \left[\beta_0 \sum_{p_0} b_{p_0} + \beta \sum_{p_s} b_{\Pi(p_s)} \eta_{p_s} U_{p_s} \prod_{e \in \partial p_s} \nu_e + K \sum_{p_t} \eta_{p_t} U_{p_t} \prod_{e \in \partial p_t} \nu_e \right] \\ &= \sum_{\{\eta_p\}} \frac{P(\{\eta_p \prod_{e \in \partial p} \nu_e\})}{\mathcal{Z}(\{\eta_p\})} \sum_{\{\sigma_{e_0}\}, \{\tau_e\}} O(\{\eta_p\}, \{\sigma_{e_0}\}, \{\tau_e\}) \\ &\times \exp \left[\beta_0 \sum_{p_0} b_{p_0} + \beta \sum_{p_s} b_{\Pi(p_s)} \eta_{p_s} U_{p_s} + K \sum_{p_t} \eta_{p_t} U_{p_t} \right] \\ &= \frac{1}{2^{3NT}} \sum_{\{\nu_e\}} \sum_{\{\eta_p\}} \frac{P(\{\eta_p \prod_{e \in \partial p} \nu_e\})}{\mathcal{Z}(\{\eta_p\})} \sum_{\{\sigma_{e_0}\}, \{\tau_e\}} O(\{\eta_p\}, \{\sigma_{e_0}\}, \{\tau_e\}) \\ &\times \exp \left[\beta_0 \sum_{p_0} b_{p_0} + \beta \sum_{p_s} b_{\Pi(p_s)} \eta_{p_s} U_{p_s} + K \sum_{p_t} \eta_{p_t} U_{p_t} \right] \\ &= \frac{1}{2^{3NT} \mathcal{Z}_{\{+\}} (2 \cosh \beta)^{NT} (2 \cosh K)^{2NT}} \sum_{\{\sigma_{e_0}\}, \{\tau_e\}, \{\eta_p\}} O(\{\eta_p\}, \{\sigma_{e_0}\}, \{\tau_e\}) \\ &\times \exp \left[\beta_0 \sum_{p_0} b_{p_0} + \beta \sum_{p_s} b_{\Pi(p_s)} \eta_{p_s} U_{p_s} + K \sum_{p_t} \eta_{p_t} U_{p_t} \right] \end{aligned} \quad (\text{S36})$$

In the third equality, we make use of the local symmetry. In the fourth equality we averaged over different $\{\nu_e\}$ since the final result $[\langle O \rangle]$ is independent of $\{\nu_e\}$. The fifth equality is obtained by noticing that:

$$\sum_{\{\nu_e\}} P(\{\eta_p \prod_{e \in \partial p} \nu_e\}) = \frac{\mathcal{Z}(\{\eta_p\})}{\mathcal{Z}_{\{+\}} (2 \cosh \beta)^{NT} (2 \cosh K)^{2NT}} \quad (\text{S37})$$

First we consider $O = W_{A_0} = \prod_{p_0 \in A_0} b_{p_0}$ which is the Wilson loop on 2-d physical lattice. Clearly, it satisfies Eq.

(S35). So we calculate its expectation value as:

$$\begin{aligned}
\langle W_{A_0} \rangle &= \frac{1}{2^{3NT} \mathcal{Z}_{\{+\}} (2 \cosh \beta)^{NT} (2 \cosh K)^{2NT}} \\
&\quad \sum_{\{\sigma_{e_0}\}, \{\tau_e\}, \{\eta_p\}} W_{A_0} \exp \left[\beta_0 \sum_{p_0} b_{p_0} + \beta \sum_{p_s} b_{\Pi(p_s)} \eta_{p_s} U_{p_s} + K \sum_{p_t} \eta_{p_t} U_{p_t} \right] \\
&= \frac{1}{\mathcal{Z}_{\{+\}} \sum_{\{\sigma_{e_0}\}} W_{A_0} \exp \left[\beta_0 \sum_{p_0} b_{p_0} \right]} = \langle W_{A_0} \rangle_{\{+\}} \\
&= \frac{(\tanh \beta_0)^{|A_0|} + (\tanh \beta_0)^{N-|A_0|}}{1 + (\tanh \beta_0)^N}
\end{aligned} \tag{S38}$$

Here $\langle \cdot \rangle_{\{+\}}$ denotes the expectation value for the pure 2-d \mathbb{Z}_2 gauge theory of physical spins σ_{e_0} , $\mathcal{Z}_{\{+\}} = \sum_{\{\sigma_{e_0}\}} \exp \left[\beta_0 \sum_{p_0} b_{p_0} \right]$. Actually, the above derivation works for any observable contains purely σ_{e_0} spins. So we conclude that the σ_{e_0} spins in SM model shown in Eq. (S29) behaves exactly the same as pure 2-d \mathbb{Z}_2 gauge theory. Specifically for the Wilson loop W_{A_0} , we find it obeys area law for any finite β_0 , same as 2-d \mathbb{Z}_2 lattice gauge theory, so the σ_{e_0} spins always stays in disordered phase.

We may also compute the internal energy, which is also invariant under the transformation shown in Eq. (S32). Given that

$$\begin{aligned}
\langle \eta_{p_s} b_{\pi(p_s)} U_{p_s} \rangle &= \frac{1}{2^{3NT} \mathcal{Z}_{\{+\}} (2 \cosh \beta)^{NT} (2 \cosh K)^{2NT}} \\
&\quad \times \sum_{\{\sigma_{e_0}\}, \{\tau_e\}, \{\eta_p\}} \eta_{p_s} b_{\pi(p_s)} U_{p_s} \exp \left[\beta_0 \sum_{p_0} b_{p_0} + \beta \sum_{p_s} b_{\Pi(p_s)} \eta_{p_s} U_{p_s} + K \sum_{p_t} \eta_{p_t} U_{p_t} \right] \\
&= \frac{1}{2^{3NT} \mathcal{Z}_{\{+\}} (2 \cosh \beta)^{NT} (2 \cosh K)^{2NT}} \sum_{\{\sigma_{e_0}\}, \{\tau_e\}} (2 \sinh \beta) (2 \cosh \beta)^{NT-1} (2 \cosh K)^{2NT} \exp \left[\beta_0 \sum_{p_0} b_{p_0} \right] \\
&= \tanh \beta,
\end{aligned} \tag{S39}$$

and similarly

$$\begin{aligned}
\langle \eta_{p_t} U_{p_t} \rangle &= \frac{1}{2^{3NT} \mathcal{Z}_{\{+\}} (2 \cosh \beta)^{NT} (2 \cosh K)^{2NT}} \\
&\quad \times \sum_{\{\sigma_{e_0}\}, \{\tau_e\}, \{\eta_p\}} \eta_{p_t} U_{p_t} \exp \left[\beta_0 \sum_{p_0} b_{p_0} + \beta \sum_{p_s} b_{\Pi(p_s)} \eta_{p_s} U_{p_s} + K \sum_{p_t} \eta_{p_t} U_{p_t} \right] \\
&= \frac{1}{2^{3NT} \mathcal{Z}_{\{+\}} (2 \cosh \beta)^{NT} (2 \cosh K)^{2NT}} \sum_{\{\sigma_{e_0}\}, \{\tau_e\}} (2 \sinh K) (2 \cosh \beta)^{NT} (2 \cosh K)^{2NT-1} \exp \left[\beta_0 \sum_{p_0} b_{p_0} \right] \\
&= \tanh K,
\end{aligned} \tag{S40}$$

we have the expression for internal energy

$$\begin{aligned}
\mathcal{U} &= \langle -\beta_0 \sum_{p_0} b_{p_0} - \beta \sum_{p_s} b_{\Pi(p_s)} \eta_{p_s} U_{p_s} - K \sum_{p_t} \eta_{p_t} U_{p_t} \rangle \\
&= -N \beta_0 \frac{\tanh \beta_0 + (\tanh \beta_0)^{N-1}}{1 + (\tanh \beta_0)^N} - NT \beta \tanh \beta - 2NTK \tanh K.
\end{aligned} \tag{S41}$$

Then consider the Wilson loop for τ_e spins $W_A = \prod_{p \in A} U_p = \prod_{e \in \partial A} \tau_e$. Note that it is not invariant under Eq.

(S32). By a similar calculation as Eq. (S36) we have:

$$\begin{aligned}
[\langle W_A \rangle] &= \sum_{\{\eta_p\}} \frac{P(\{\eta_p\})}{\mathcal{Z}(\{\eta_p\})} \sum_{\{\sigma_{e_0}\}, \{\tau_e\}} W_A \exp \left[\beta_0 \sum_{p_0} b_{p_0} + \beta \sum_{p_s} b_{\Pi(p_s)} \eta_{p_s} U_{p_s} + K \sum_{p_t} \eta_{p_t} U_{p_t} \right] \\
&= \sum_{\{\eta_p\}} \frac{P(\{\eta_p \prod_{e \in \partial p} \nu_e\})}{\mathcal{Z}(\{\eta_p\})} \sum_{\{\sigma_{e_0}\}, \{\tau_e\}} W_A \prod_{e \in \partial A} \nu_e \\
&\quad \times \exp \left[\beta_0 \sum_{p_0} b_{p_0} + \beta \sum_{p_s} b_{\Pi(p_s)} \eta_{p_s} U_{p_s} + K \sum_{p_t} \eta_{p_t} U_{p_t} \right] \\
&= \frac{1}{2^{3NT}} \sum_{\{\nu_e\}} \sum_{\{\eta_p\}} \frac{P(\{\eta_p \prod_{e \in \partial p} \nu_e\}) \prod_{e \in \partial A} \nu_e}{\mathcal{Z}(\{\eta_p\})} \sum_{\{\sigma_{e_0}\}, \{\tau_e\}} W_A \\
&\quad \times \exp \left[\beta_0 \sum_{p_0} b_{p_0} + \beta \sum_{p_s} b_{\Pi(p_s)} \eta_{p_s} U_{p_s} + K \sum_{p_t} \eta_{p_t} U_{p_t} \right] \\
&= \frac{1}{2^{3NT} \mathcal{Z}_{\{+\}} (2 \cosh \beta)^{NT} (2 \cosh K)^{2NT}} \sum_{\{\eta_p\}} \mathcal{Z}(\{\eta_p\}) \langle W_A \rangle^2 \\
&= [\langle W_A \rangle^2]
\end{aligned} \tag{S42}$$

The result $[\langle W_A \rangle] = [\langle W_A \rangle^2]$ signifies the absence of gauge glass phase ($[\langle W_A \rangle] = 0$, $[\langle W_A \rangle^2] > 0$) on the Nishimori line [7].

In addition, one may find that the modified Wilson loop $W_A \prod_{p \in A} \eta_p$ is invariant under local symmetry. It can be calculated as

$$\begin{aligned}
[\langle W_A \prod_{p \in A} \eta_p \rangle] &= \frac{1}{2^{3NT} \mathcal{Z}_{\{+\}} (2 \cosh \beta)^{NT} (2 \cosh K)^{2NT}} \\
&\quad \times \sum_{\{\sigma_{e_0}\}, \{\tau_e\}, \{\eta_p\}} W_A \prod_{p \in A} \eta_p \exp \left[\beta_0 \sum_{p_0} b_{p_0} + \beta \sum_{p_s} b_{\Pi(p_s)} \eta_{p_s} U_{p_s} + K \sum_{p_t} \eta_{p_t} U_{p_t} \right] \\
&= \frac{1}{2^{3NT} \mathcal{Z}_{\{+\}} (2 \cosh \beta)^{NT} (2 \cosh K)^{2NT}} \sum_{\{\sigma_{e_0}\}, \{\tau_e\}} \exp \left[\beta_0 \sum_{p_0} b_{p_0} \right] \\
&\quad \times \left(\prod_{p_s \in A_s} \sum_{\eta_{p_s}} \eta_{p_s} U_{p_s} \exp [\beta b_{\Pi(p_s)} \eta_{p_s} U_{p_s}] \prod_{p_s \notin A_s} \sum_{\eta_{p_s}} \exp [\beta b_{\Pi(p_s)} \eta_{p_s} U_{p_s}] \right) \\
&\quad \times \left(\prod_{p_t \in A_t} \sum_{\eta_{p_t}} \eta_{p_t} U_{p_t} \exp [K \eta_{p_t} U_{p_t}] \prod_{p_t \notin A_t} \sum_{\eta_{p_t}} \exp [K \eta_{p_t} U_{p_t}] \right) \\
&= \frac{1}{2^{3NT} \mathcal{Z}_{\{+\}} (2 \cosh \beta)^{NT} (2 \cosh K)^{2NT}} \sum_{\{\sigma_{e_0}\}, \{\tau_e\}} \exp \left[\beta_0 \sum_{p_0} b_{p_0} \right] \\
&\quad \times \left(\prod_{p_s \in A_s} b_{\pi(p_s)} \right) (2 \sinh \beta)^{|A_s|} (2 \cosh \beta)^{NT - |A_s|} (2 \sinh K)^{|A_t|} (2 \cosh K)^{2NT - |A_t|} \\
&\quad \langle W_{\Pi(A)} \rangle_{\{+\}} (\tanh \beta)^{|A_s|} (\tanh K)^{|A_t|}
\end{aligned} \tag{S43}$$

Here A_s and A_t denote the sets of spacelike plaquettes and timelike plaquettes contained in A respectively. Π is the projection onto physical lattice, see Fig. S9. This expression reveals that τ_e 's and σ_e 's are correlated and their Wilson loops somehow depend on each other. However, the modified Wilson loop $W_A \prod_{p \in A} \eta_p$ cannot serve as the correct order parameter for the error threshold.

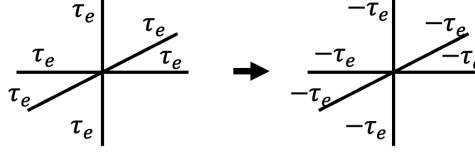


FIG. S7. Example of 1-form symmetry operation. The τ_e spins on a closed surface (surrounding the center vertex in this figure) are flipped.

SIV. LOW TEMPERATURE EXPANSION

The ordered (deconfinement) phase is expected to exist at the exact zero temperature point (on the Nishimori line) $\beta_0, \beta, K \rightarrow +\infty$. Near the zero temperature point, we may perform a low-temperature expansion for Wilson loops to show if the ordered phase still persists to some finite temperature. Assume $e^{-\beta_0}$, $e^{-\beta}$, e^{-K} are of the same order, we expand $[\langle W_A \rangle]$ up to the order $e^{-4\beta}$ following the method discussed in Ref. [3].

We first perform the expansion for the disorder probability $P(\{\eta_p\})$. Through the expression of $P(\{\eta_p\})$

$$P(\{\eta_e\}) = \frac{2^{N+1} \sum_{\{b_{p_0}\}} \frac{1+\prod_{p_0} b_{p_0}}{2} \exp \left[\beta_0 \sum_{p_0} b_{p_0} + \beta \sum_{p_s} b_{\Pi(p_s)} \eta_{p_s} + K \sum_{p_t} \eta_{p_t} \right]}{\mathcal{Z}_{\{+\}} \prod_t [(2 \cosh \beta)^N (2 \cosh K)^{2N}]}. \quad (\text{S44})$$

We notice that the zeroth order is contributed by the configuration that all b_{p_0} and η_p are equal to +1. The order $e^{-2\beta}$ is given by flipping one of the η_{p_s} to -1. The order $e^{-4\beta}$ is given by flipping any two of the η_{p_s} or flipping two of b_{p_0} s. Note that the parity of $\{b_{p_0}\}$ configuration must be even. Then we find that the numerator is expanded as

$$2^{N+1} E^{N\beta_0 + NT\beta + 2NTK} \left[\delta_{\{+\}} + e^{-2K} \sum_{p_t} \delta_{\{p_t\}} + e^{-2\beta} \sum_{p_s} \delta_{\{p_s\}} \right. \\ \left. + e^{-4K} \sum_{(p_t, p'_t)} \delta_{\{(p_t, p'_t)\}} + e^{-4\beta} \sum_{(p_s, p'_s)} \delta_{\{(p_s, p'_s)\}} + e^{-2\beta-2K} \sum_{(p_s, p_t)} \delta_{\{(p_s, p_t)\}} + e^{-4\beta_0} \sum_{(p_0, p'_0)} \delta_{\{\Pi^{-1}(p_0, p'_0)\}} \right]. \quad (\text{S45})$$

Here (p, p') denotes a pair of different plaquettes. For example (p_s, p'_s) denotes a pair of spacelike plaquettes and the summation $\sum_{(p_s, p'_s)}$ is taken on all such pairs. We have used a simplified notation for the Kronecker delta symbol. δ_+ means that all the η_{p_s} are fixed to be +1, $\delta_+ = \prod_p \delta_{\eta_p, +}$. δ_p denotes that η_p on the given plaquette p is flipped to -1, $\delta_p = \delta_{\eta_p, -} \prod_{p' \neq p} \delta_{\eta_{p'}, +}$, and similar for $\delta_{(p, p')}$, $\delta_{(p, p')} = \delta_{\eta_p, -} \delta_{\eta_{p'}, -} \prod_{p'' \neq p, p'} \delta_{\eta_{p''}, +}$. Finally $\delta_{\Pi^{-1}(p_0, p'_0)}$ means that all the spacelike plaquettes whose projection on the physical lattice is p_0 or p'_0 are set to be -1, $\delta_{\Pi^{-1}(p_0, p'_0)} = \prod_{p_s | \Pi(p_s) = p_0} \delta_{\eta_{p_s}, -} \prod_{p'_s | \Pi(p'_s) = p'_0} \delta_{\eta_{p'_s}, -} \prod_{p''_s | \Pi(p''_s) \neq p_0, p'_0} \delta_{\eta_{p''_s}, +}$. The number of integer times T should be sent to $+\infty$ at the end of the calculation. Combined with the denominator, we arrive at a perturbative expression for disorder probability

$$P(\{\eta_p\}) \simeq [1 - (1 - 2NTe^{-2K} - NTe^{-2\beta}) (2NTe^{-2K} + NTe^{-2\beta}) \\ - \left(\binom{2NT}{2} e^{-4K} + \binom{NT}{2} e^{-4\beta} + 2(NT)^2 e^{-2K-2\beta} + \binom{N}{2} e^{-4\beta_0} \right) \delta_{\{+\}} \\ + (1 - 2NTe^{-2K} - NTe^{-2\beta}) \left[e^{-2K} \sum_{p_t} \delta_{\{p_t\}} + e^{-2\beta} \sum_{p_s} \delta_{\{p_s\}} \right] \\ + e^{-4K} \sum_{(p_t, p'_t)} \delta_{\{(p_t, p'_t)\}} + e^{-4\beta} \sum_{(p_s, p'_s)} \delta_{\{(p_s, p'_s)\}} + e^{-2\beta-2K} \sum_{(p_s, p_t)} \delta_{\{(p_s, p_t)\}} + e^{-4\beta_0} \sum_{(p_0, p'_0)} \delta_{\{\Pi^{-1}(p_0, p'_0)\}}]. \quad (\text{S46})$$

Then we analyze the ensemble-averaged value for the interaction configurations that appeared in the above expression. Keeping in mind the fact that the interaction term U_p and Wilson loop W_A are both invariant under 1-form symmetry operations which flip the spins on a 2-d surface on the dual lattice as in Fig. S7, when performing the spin configuration summation for the lowest few orders we extract a factor of 1-form symmetry operation numbers \mathcal{N}_1 and evaluate the coefficient for each order on an equivalent class of spin configurations module 1-form symmetry.

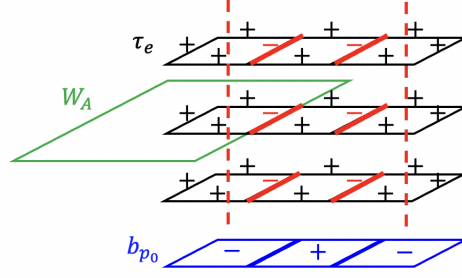


FIG. S8. Spin configuration when two b_{p_0} are flipped. The $\{b_{p_0}\}$ configuration is shown on the blue lattice. The timelike plaquettes are omitted for explicitness. The two red dashed strings represent the locations of -1 plaquette interaction caused by $b_{\Pi(p_s)} = -1$, and their energy cost can be eliminated by flipping the spins on the solid red edges.

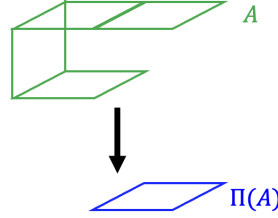


FIG. S9. The action of projection Π on surface A . The above surface lies inside 3-d spacetime and its projection on 2-d space is shown below. Their boundaries correspondingly are Wilson loops in 3-d spacetime and 2-d space.

First, consider the case all $\eta_p = +1$, and we want to compute

$$\langle W_A \rangle_{\{+\}} = \frac{1}{\mathcal{Z}(\{+\})} \sum_{\{\sigma_{e_0}\}, \{\tau_e\}} \left(\prod_{e \in \partial A} \tau_e \right) \exp \left[\beta_0 \sum_{p_0} b_{p_0} + \beta \sum_{p_s} b_{\Pi(p_s)} U_{p_s} + K \sum_{p_t} U_{p_t} \right]. \quad (\text{S47})$$

The 0th order is contributed by the ground states, and a representative spin configuration is that all $\tau_e = +1$ and $b_{p_0} = +1$. It leads to the term:

$$\mathcal{N}_1 2^{N+1} e^{N\beta_0 + NT\beta + 2NTK} \quad (\text{S48})$$

in both the numerator and denominator. Now if we flip one of the τ_e spins to -1 , it increases the energy of four neighbor plaquettes and results in a term of order $e^{-8\beta}$, which is not included in our expansion. However, if we flip two b_{p_0} s, this only yields a term of order $e^{-4\beta_0}$ in the infinite boundary condition case. When two b_{p_0} s are flipped, it leads to -1 interactions on two strings of spacelike plaquettes corresponding to the position of b_{p_0} , as shown in S8, and it should cost infinite energy. However, the energy cost can be eliminated by the local symmetry transformation in Eq. (S32). The two strings can be viewed as merged together by setting the τ_e spins on the surface connecting them to -1 . Deformation of the surface is nothing but a 1-form symmetry operation and has already been mod out. Combining both the b_{p_0} configuration and the τ_e spin configuration, the total energy cost is just $4\beta_0$. Now consider the value of the Wilson loop. During the process of merging two strings together, if they cross the Wilson loop for odd times, then exactly one of the spins on the boundary of region A will be flipped to -1 . So the value of the Wilson loop for that configuration is -1 . But if the Wilson loop is crossed for even times, it still gets $+1$. The total contribution of order $e^{-4\beta_0}$ is obtained by summing all the choices for flipping two b_{p_0} s, which contains $\binom{N}{2}$ terms. By counting the number of odd time crosses, we obtain the expression for an additional term in the numerator

$$\left(\binom{N}{2} - 2|\Pi(A)|(N - |\Pi(A)|) \right) e^{-4\beta_0}. \quad (\text{S49})$$

Here we define $\Pi(A)$ as the projection of region A on the spacelike 2-d lattice module \mathbb{Z}_2 . The timelike plaquettes are dropped under projection, and an even number of spacelike plaquettes on the same space position also leads to zero, as in Fig. S9. For denominator, the new term is just $\binom{N}{2} e^{-4\beta_0}$. So the expansion of $\langle W_A \rangle_{\{+\}}$ is evaluated as

$$\begin{aligned} \langle W_A \rangle_{\{+\}} &\simeq \frac{\mathcal{N}_1 2^{N+1} e^{N\beta_0 + NT\beta + 2NTK} \left[1 + \left(\binom{N}{2} - 2|\Pi(A)|(N - |\Pi(A)|) \right) e^{-4\beta_0} \right]}{\mathcal{N}_1 2^{N+1} e^{N\beta_0 + NT\beta + 2NTK} \left[1 + \binom{N}{2} e^{-4\beta_0} \right]} \\ &\simeq 1 - 2|\Pi(A)|(N - |\Pi(A)|) e^{-4\beta_0}. \end{aligned} \quad (\text{S50})$$

From this expression, we can roughly say that $\langle W_A \rangle_{\{+\}}$ decays with respect to the spacelike area.

Now we evaluated the Wilson loop configurations that only one η_p is flipped. Suppose a timelike plaquette p_t is flipped. Now the ground state energy is $2K$ higher than the previous all $\eta_p = +1$ case and the ground state spin configuration remains the same, which is all $\tau_e = +1$. The lowest excitation is caused by flipping one of the spins at the boundary of p_t , which has the extra energy $4K$. It eventually results in terms of order e^{-4K} . Notice that the probability of $\eta_{p_t} = -1$ is already of the order e^{-2K} , so we only need to concern about the ground state in our expansion, and it leads to

$$\langle W_A \rangle_{\{p_t\}} \simeq 1. \quad (\text{S51})$$

Similarly, for the spacelike plaquette flipping, we also have

$$\langle W_A \rangle_{\{p_s\}} \simeq 1. \quad (\text{S52})$$

Then we consider the configuration where two η_p s are flipped. Notice that only the ground state contribution survives in our expansion since the probability is already of the order $e^{-4\beta}$. We the two flipped η_p s do not contact each other, the representative spin configuration for ground state is still all $\tau_e = +1$ and only those two plaquettes where $\eta_p = -1$ have energy costs. But when the two flipped plaquettes are nearest neighbors, there will be two degenerate (ignoring the energetic difference between β and K) configurations that both have energy costs on two plaquettes. They are distinguished by whether the contacting edge of the two plaquettes is flipped to -1 . If the contacting edges lie on the Wilson loop, then summing the two degenerate configurations leads to $W_A = 0$. So assume the two flipped plaquettes are p and p' , then the Wilson loop takes the value

$$\langle W_A \rangle_{\{(p,p')\}} \simeq 1 - |\partial A \cap \partial p \cap \partial p'|. \quad (\text{S53})$$

If the two plaquettes and the Wilson loop intersect at one edge, $|\partial A \cap \partial p \cap \partial p'|$ takes 1. Otherwise, it takes 0. Consider the disorder summation of these configurations. Each edge connects to 4 plaquettes, yielding 6 pairs of nearest-neighbor plaquettes. By noticing that each timelike edge is associated with 6 pairs of timelike plaquettes while each spacelike edge is associated with a pair of timelike plaquettes, a pair of spacelike plaquettes and 4 combinations of spacelike and timelike plaquettes, we find that

$$\begin{aligned} e^{-4\beta} \sum_{(p_s, p'_s)} \langle W_A \rangle_{\{(p_s, p'_s)\}} &\simeq e^{-4\beta} \left(\binom{NT}{2} - |\partial A|_s \right) \\ e^{-4K} \sum_{(p_t, p'_t)} \langle W_A \rangle_{\{(p_t, p'_t)\}} &\simeq e^{-4K} \left(\binom{2NT}{2} - |\partial A|_s - 6|\partial A|_t \right) \\ e^{-2\beta-2K} \sum_{(p_t, p_s)} \langle W_A \rangle_{\{(p_t, p_s)\}} &\simeq e^{-2\beta-2K} (2(NT)^2 - 4|\partial A|_s). \end{aligned} \quad (\text{S54})$$

Here $|\partial A|_s$ denotes the number of spacelike edges in ∂A and $|\partial A|_t$ is the number of timelike edges in ∂A .

Finally we turn to the configuration denoted as $\{\Pi^{-1}(p_0, p'_0)\}$, which means all the spacelike interactions η_{p_s} along the timelike strings with the same space position as p_0 or p'_0 are flipped. In this case, a similar argument while evaluating Eq. (S50) could be applied. The two timelike strings are merged together by setting the spins in the interval to -1 , which gives us the ground state configuration. So the leading order of the Wilson loop is

$$\langle W_A \rangle_{\{\Pi^{-1}(p_0, p'_0)\}} \simeq \pm 1. \quad (\text{S55})$$

which takes -1 when only one of the p_0 and p'_0 stays in $\Pi(A)$ and takes $+1$ otherwise. Performing the disorder summation, we find that

$$e^{-4\beta_0} \sum_{(p_0, p'_0)} \langle W_A \rangle_{\{\Pi^{-1}(p_0, p'_0)\}} \simeq e^{-4\beta_0} \left(\binom{N}{2} - 2|\Pi(A)|(N - |\Pi(A)|) \right). \quad (\text{S56})$$

Putting all these stuff together, we arrive at the low-temperature expansion for the Wilson loop

$$[\langle W_A \rangle] \simeq 1 - 4|\Pi(A)|(N - |\Pi(A)|)e^{-4\beta_0} - |\partial A|_s (e^{-4\beta} + e^{-4K} + 4e^{-2\beta-2K}) - 6|\partial A|_t e^{-4K} \\ \simeq \exp [-4|\Pi(A)|(N - |\Pi(A)|)e^{-4\beta_0} - |\partial A|_s (e^{-4\beta} + e^{-4K} + 4e^{-2\beta-2K}) - 6|\partial A|_t e^{-4K}]. \quad (\text{S57})$$

Note that the factor $|\Pi(A)|(N - |\Pi(A)|)$ appears because our space manifold is a closed surface. The result is natural to be symmetric between $\Pi(A)$ and the 2-d complement of $\Pi(A)$. We also notice that the number of integer time T automatically vanishes in these expressions so they already suit the case $T \rightarrow +\infty$.

From Eq. (S57) we can see that once the initial state preparation suffers from imperfect measurement, the scaling behavior of Wilson loops becomes anisotropic for space and time direction. For a Wilson loop A purely containing spacelike plaquettes, we have

$$[\langle W_A \rangle] \simeq \exp [-4|A|(N - |A|)e^{-4\beta_0} - |\partial A| (e^{-4\beta} + e^{-4K} + 4e^{-2\beta-2K})]. \quad (\text{S58})$$

For large enough N and large enough Wilson loop satisfying $|A| < N/2$, the area law decaying term dominates and the perimeter term can be ignored. So we conclude that the spacelike Wilson loop always decays with respect to the area at finite temperature even when the temperature is sufficiently low. Equivalently we can say that once the initial state is prepared under imperfect measurement, the spacelike Wilson loop always obeys area law. However, for a timelike Wilson loop, we will get:

$$[\langle W_A \rangle] \simeq \exp [- (e^{-4\beta} + e^{-4K} + 4e^{-2\beta-2K}) |\partial A|_s - 6e^{-4K} |\partial A|_t]. \quad (\text{S59})$$

so there will be a finite temperature phase for it to exhibit perimeter law scaling.

As we mentioned in the main text, the subtlety of Eq. (S57) is that we cannot directly take the thermodynamic limit $N \rightarrow \infty$. However, we may infer the thermodynamic result in analogy to the 2-d \mathbb{Z}_2 gauge theory. We may expand the Wilson loop for 2-d \mathbb{Z}_2 gauge theory Eq. (S38) also up to $e^{-4\beta_0}$:

$$\langle W_{A_0} \rangle_{\{+\}} \simeq 1 - 2|A_0|(N - |A_0|)e^{-4\beta_0}. \quad (\text{S60})$$

Compared with Eq. (S57) we find an approximate relation under low temperatures:

$$[\langle W_A \rangle] \simeq \langle W_{\Pi(A)} \rangle_{\{+\}}^2 \exp [-|\partial A|_s (e^{-4\beta} + e^{-4K} + 4e^{-2\beta-2K}) - 6|\partial A|_t e^{-4K}]. \quad (\text{S61})$$

In this expression $[\langle W_A \rangle]$ is a Wilson loop for τ_e spins and it relates to a Wilson loop $\langle W_{\Pi(A)} \rangle_{\{+\}}$ for σ_{e_0} spins in the 2-d physical lattice. Recall that $\langle \cdot \rangle_{\{+\}}$ denotes the expectation value for 2-d \mathbb{Z}_2 gauge theory $\mathcal{Z}_{\{+\}} = \sum_{\{\sigma_{e_0}\}} \exp(\beta_0 \sum_{p_0} b_{p_0})$. The expression in Eq. (S61) absorbs the size of space N and we expect it to valid under the thermodynamic limit. Turn back to Eq. (S38). If we take the $N \rightarrow +\infty$ limit first (keeping A_0 a finite region) and then perform low-temperature expansion, we arrive at

$$\langle W_{A_0} \rangle_{\{+\}} \simeq 1 - 2|A_0|e^{-2\beta_0} + 2|A_0|^2 e^{-4\beta_0}. \quad (\text{S62})$$

The difference between Eq. (S60) and Eq. (S62) arise from the criticality at zero temperature $\beta_0 = +\infty$. The $e^{-2\beta_0}$ term exhibit a discontinuity at zero temperature, which leads to the non-commuting of $N \rightarrow +\infty$ limit and $\beta_0 \rightarrow +\infty$ limit. A similar critical behavior should be found in $[\langle W_A \rangle]$. If the thermodynamic limit is taken before the low-temperature expansion, we infer that (not a rigorous proof)

$$[\langle W_A \rangle] \simeq \exp [-4|\Pi(A)|e^{-2\beta_0} + 4|\Pi(A)|^2 e^{-4\beta_0} - |\partial A|_s (e^{-4\beta} + e^{-4K} + 4e^{-2\beta-2K}) - 6|\partial A|_t e^{-4K}]. \quad (\text{S63})$$

In all, we expect that spacelike Wilson loops still decay with respect to area under the thermodynamic limit. Another way to think about the area law of spacelike Wilson loops when $N \rightarrow +\infty$ is to reconsider an open boundary condition at the spacelike directions and take an infinitely large system size before calculating the low-temperature expansion. Then an odd number of flipped b_{p_0} is allowed since we can send one in a pair of b_{p_0} 's to the infinity and eliminate it. Thus up to the leading order we have $[\langle W_A \rangle] \simeq \exp [-4|\Pi(A)|e^{-2\beta_0}]$. Although this open boundary condition does not correspond to any QEC procedure, we expect that the phase structure of the SM model does not depend on the choice of spacelike boundary conditions, and the expectation values of the order parameter for both the two kinds of boundary conditions should match under the thermodynamic limit.

In addition, Eq. S61 implies that the area law behavior of spacelike Wilson loops is controlled by the finite temperature disordered phase of the 2-d physical σ_{e_0} spins. Note that the area law behavior of the Wilson loop

$\langle W_{A_0} \rangle_{\{+\}}$ is used in Ref. [1, 2] to argue the absence of long-range entanglement in the imperfect initial state. So in some sense, Eq. (S61) relates the inability of correcting measurement errors to the absence of long-range entanglement through σ_{e_0} spins.

-
- [1] G.-Y. Zhu, N. Tantivasadakarn, A. Vishwanath, S. Trebst, and R. Verresen, Nishimori’s cat: stable long-range entanglement from finite-depth unitaries and weak measurements (2022), [arXiv:2208.11136 \[quant-ph\]](#).
 - [2] J. Y. Lee, W. Ji, Z. Bi, and M. P. A. Fisher, Decoding measurement-prepared quantum phases and transitions: from ising model to gauge theory, and beyond (2022), [arXiv:2208.11699 \[cond-mat.str-el\]](#).
 - [3] J. B. Kogut, An introduction to lattice gauge theory and spin systems, *Rev. Mod. Phys.* **51**, 659 (1979).
 - [4] S. Elitzur, Impossibility of spontaneously breaking local symmetries, *Phys. Rev. D* **12**, 3978 (1975).
 - [5] E. Dennis, A. Kitaev, A. Landahl, and J. Preskill, Topological quantum memory, *Journal of Mathematical Physics* **43**, 4452 (2002).
 - [6] H. Nishimori, Internal Energy, Specific Heat and Correlation Function of the Bond-Random Ising Model, *Progress of Theoretical Physics* **66**, 1169 (1981).
 - [7] C. Wang, J. Harrington, and J. Preskill, Confinement-higgs transition in a disordered gauge theory and the accuracy threshold for quantum memory, *Annals of Physics* **303**, 31 (2003).